Biophysical Journal
Article

Biophysical Society

Length matters: Functional flip of the short TatA transmembrane helix

Eva R. Stockwald,[1] Lena M. E. Steger,[2] Stefanie Vollmer,[1] Christina Gottselig,[1] Stephan L. Grage,[2] Jochen Bürck,[2] Sergii Afonin,[2] Julia Fröbel,[3] Anne-Sophie Blümmel,[3] Julia Setzler,[4] Wolfgang Wenzel,[4] Torsten H. Walther,[2,*] and Anne S. Ulrich[1,2,*]

[1]Karlsruhe Institute of Technology (KIT), Institute of Organic Chemistry, Karlsruhe, Germany; [2]Karlsruhe Institute of Technology (KIT), Institute of Biological Interfaces (IBG-2), Karlsruhe, Germany; [3]University of Freiburg, Institute of Biochemistry and Molecular Biology, Freiburg, Germany; and [4]Karlsruhe Institute of Technology (KIT), Institute of Nanotechnology, Karlsruhe, Germany

ABSTRACT The twin arginine translocase (Tat) exports folded proteins across bacterial membranes. The putative pore-forming or membrane-weakening component ($TatA_d$ in *B. subtilis*) is anchored to the lipid bilayer via an unusually short transmembrane α-helix (TMH), with less than 16 residues. Its tilt angle in different membranes was analyzed under hydrophobic mismatch conditions, using synchrotron radiation circular dichroism and solid-state NMR. Positive mismatch (introduced either by reconstitution in short-chain lipids or by extending the hydrophobic TMH length) increased the helix tilt of the TMH as expected. Negative mismatch (introduced either by reconstitution in long-chain lipids or by shortening the TMH), on the other hand, led to protein aggregation. These data suggest that the TMH of TatA is just about long enough for stable membrane insertion. At the same time, its short length is a crucial factor for successful translocation, as demonstrated here in native membrane vesicles using an in vitro translocation assay. Furthermore, when reconstituted in model membranes with negative spontaneous curvature, the TMH was found to be aligned parallel to the membrane surface. This intrinsic ability of TatA to flip out of the membrane core thus seems to play a key role in its membrane-destabilizing effect during Tat-dependent translocation.

SIGNIFICANCE Transport of fully folded proteins across the lipid membrane barrier—requiring a large opening without uncontrolled ion leakage—is a remarkable capability of the twin arginine translocase. This protein complex is present in archaea, bacteria, and plant thylakoids. It has been thoroughly investigated since its discovery ~30 years ago, but its functional mechanism and interactions with the lipid matrix remain elusive. The putative pore-forming or membrane-weakening component is the transmembrane protein TatA, which has a single, exceptionally short transmembrane helix. Our study suggests that this helix has an intrinsic ability to flip out of the hydrophobic membrane core, which seems to be functionally relevant in the Tat-dependent translocation mechanism.

INTRODUCTION

The Tat-dependent translocase is capable of transporting large proteins in their native folded state across bacterial and thylakoid membranes, driven only by the proton motive force, as reviewed in (1–8). In most Gram-negative bacteria, the Tat translocase is composed of the integral membrane proteins TatA, TatB, and TatC (9–11), whereas in many Gram-positive bacteria the minimal Tat translocase consists of TatA and TatC only (7). In *B. subtilis,* there exist at least two substrate-specific minimal TatA/TatC translocases (12), of which the $TatA_d/TatC_d$ system is responsible for the secretion of the enzyme phosphodiesterase PhoD under phosphate deficiency (13). In such minimal translocases, TatA has been suggested to cover also the function of the absent TatB component (14,15). Based on mutation and interaction studies, TatC is known to act as a receptor to recognize and bind the cargo protein via its Arg-Arg-containing signal peptide (16–20). Numerous experimental findings have shown that TatC can form a functional TatBC complex by associating with TatB, which acts as a mediator between TatA and TatC (17,21–23). In the early literature, TatA was suggested to constitute the translocation pore per se, allowing for a large and variable diameter to appropriately fit the size of any corresponding protein cargo

Submitted September 26, 2022, and accepted for publication December 12, 2022.

*Correspondence: torsten.walther@kit.edu or anne.ulrich@kit.edu

Eva R. Stockwald and Lena M.E. Steger contributed equally to this work.

Editor: Marta Filizola.

https://doi.org/10.1016/j.bpj.2022.12.016

(24). This interpretation was based on the findings of its high molar excess over TatC (25) and its tendency for homo-oligomerization (14,24,26–29). More recently, it became clear that the Tat(B)/C complex also participates actively in the translocation site (30,31).

Structural data on the key components of the translocase is required as a basis for understanding any functional mechanism in detail, and the three-dimensional (3D) structures of all individual Tat proteins have been resolved (32–38). The crystal structure of TatC from the hyperthermophilic bacterium *A. aeolicus* shows a bundle of six transmembrane helices arranged like a baseball glove (35, 36). TatA and TatB both consist of an N-terminal transmembrane α-helix (TMH), a surface-aligned amphiphilic α-helix (APH), and an unstructured C-terminal region, as revealed by circular dichroism (CD) and NMR spectroscopy (32,33,37,39–41). TatA and TatB differ in the length of their C-terminal region, and TatB also has a significantly longer APH (37,42). Based on a charge zipper motif in the TatA primary sequence, we have postulated that the membrane-bound TatA proteins can homo-oligomerize into a long chain via a network of intra- and intermolecular salt bridges between them (29).

However, the molecular details of the translocation process remain largely unknown. Several mechanisms for the TatA-induced membrane permeabilization step have been suggested, such as a "trapdoor" mechanism (24,43–46), where the APH segment flips into the lipid bilayer to open up a pore with a hydrophilic lining. Another proposed mechanism involves "membrane weakening," as originally postulated by Brüser and co-workers. (47,48) and supported by Rodriguez et al. (34). Whichever mechanism applies, it must involve many units of TatA, besides an interface with TatC. In this context, it is striking to realize that the transmembrane helix of TatA is exceptionally short compared with other membrane proteins. Based on D_2O exchange observed by liquid-state NMR in micelles, we have shown previously that the hydrophobic stretch of the *B. subtilis* $TatA_d$ TMH extends from Leu_{10} to Phe_{21}, spanning merely 12 residues (32). This sequence was shielded inside a hydrophobic SDS micelle core, whereas the backbone amide signals of Gly_9 and Gly_{22} disappeared within minutes after D_2O addition due to H/D exchange, implying that they lie in the polar interphase region of the SDS micelle. The TMH region of $TatA_d$ from *B. subtilis* is terminated on both sides by proline-flanking glycine residues (Pro_8Gly_9 and $Gly_{22}Pro_{23}$), which are typically known to induce a break in an α-helix (49). Altogether, this yields a contiguous transmembrane helix of at most 16 amino acids in length (see Table 1). The well-studied *E. coli* TatA protein possesses a TMH with an equally short hydrophobic stretch of 12 residues from Leu_9 to Phe_{20}, although it is not flanked by proline residues (see Table 1). Nonetheless, it starts with Trp, a so-called flanking residue that is typically found at the ends of transmembrane segments in the interphase region of the lipid bilayer (50–52). The same helix dimensions are also seen in other TatA proteins (see Fig. S1). Two recent publications have indeed highlighted the functional importance of the short TatA TMH and the role of the resulting hydrophobic mismatch in the process of Tat-dependent translocation (53,54).

To further understand the significance of the short length of the TMH, we have systematically studied the membrane alignment of *B. subtilis* $TatA_d$ as a function of hydrophobic mismatch and different lipid bilayer curvature. Besides varying the lipid matrix, we also examined several $TatA_d$ variants with either an extended or a shortened TMH. All recombinant proteins were reconstituted in phosphatidylcholine bilayers with different membrane thickness (and rather neutral curvature), as well as in branched phytanoyl bilayers that have a highly negative curvature. The alignment of the two constituent TatA helices (TMH and APH) in the membrane was determined using a combination of synchrotron radiation circular dichroism (SRCD) and solid-state nuclear magnetic resonance, performed on the same type of macroscopically oriented membrane samples. Furthermore, with an in vitro translocation assay, we investigated the effect of an elongated TMH on the translocation efficiency, to connect the biophysical observations on model membranes with a functionally active native membrane system.

RESULTS

In previous solid-state ^{15}N-NMR studies (32,41), we noted that the full-length $TatA_d$ protein (70 amino acids) in macroscopically oriented samples yields spectra with poor resolution, due to the disordered C-terminal region from Ser_{46} to Gly_{70} (40). A structural interpretation of these spectral line shapes is awkward and gets further complicated by the intrinsic tendency of $TatA_d$ to homo-oligomerize (14,28,55). Therefore, we have used in the present studies the same C-terminally truncated $TatA_{2\text{-}45}$ as before (32,40,41). Consisting only of the TMH and the APH this truncated construct can be regarded as a representative model of the $TatA_d$ monomer as it retains the same secondary structure as the wild-type protein (32,40,41).

Influence of bilayer thickness on the secondary structure of $TatA_{2\text{-}45}$

As a first step, we selected a series of lipids with different acyl chain lengths to reconstitute TatA in model membranes with varying thickness under biologically relevant liquid-crystalline conditions. To systematically examine the influence of bilayer thickness on the α-helical folding of $TatA_{2\text{-}45}$, we used phosphatidylcholine lipids with chain lengths ranging from 8 to 24 carbon atoms. These lipids and their physical properties are summarized in Table 2. We employed a series of saturated lipids only from DOcPC (diC 8:0) to DMPC (diC 14:0) because the elevated phase transition

TABLE 1 Primary sequences of the TatA constructs

Wild type sequences	
B. subtilis $TatA_d$	MFSNIGI**PG**LILIFVIALIIF**GP**SKL*PEIGRAAGRTLLEFKSATK*SLVSGDEKEEKS AELTAVKQDKNAG
E. coli TatA	MGGISI**WQ**LLIIAVIVVLLF**G**TKK*LGSIGSDLGASIKGFKKAMS*DDEPKQDKTSQ DADFTAKTIADKQADTNQEQAKTEDAKRHDKEQV
***B. subtilis* $TatA_d$ variants**	
$TatA_{2\text{-}45}$	FSNIGI**PG**LILIFVIALIIF**GP**SKL*PEIGRAAGRTLLEFKSATK*
$TatA_{2\text{-}45}$ ΔLIL	FSNIGI**PG**LIL**IF**VIALIIF**GP**SKL*PEIGRAAGRTLLEFKSATK*
$TatA_{2\text{-}45}$ LAL	FSNIGI**PG**LIL**LAL**IFVIALIIF**GP**SKL*PEIGRAAGRTLLEFKSATK*
$TatA_{2\text{-}45}$ LALAL	FSNIGI**PG**LIL**LALAL**IFVIALIIF**GP**SKL*PEIGRAAGRTLLEFKSATK*
$TatA_{2\text{-}45}$ LALALAL	FSNIGI**PG**LIL**LALALAL**IFVIALIIF**GP**SKL*PEIGRAAGRTLLEFKSATK*
$TatA_{2\text{-}45}$ F_2D	DSNIGI**PG**LILIFVIALIIF**GP**SKL*PEIGRAAGRTLLEFKSATK*
$TatA_{2\text{-}45}$ F_2DI_7D	DSNIGD**PG**LILIFVIALIIF**GP**SKL*PEIGRAAGRTLLEFKSATK*
E. coli TatA variants	
TatA LAL	MGGISI**WQ**LLI**LAL**IAVIVVLLF**G**TKK*LGSIGSDLGASIKGFKKAMS*DDEPKQDK TSQDADFTAKTIADKQADTNQEQAKTEDAKRHDKEQV
TatA LALA	MGGISI**WQ**LLI**LALA**IAVIVVLLF**G**TKK*LGSIGSDLGASIKGFKKAMS*DDEPKQD KTSQDADFTAKTIADKQADTNQEQAKTEDAKRHDKEQV
TatA LALALAL	MGGISI**WQ**LLI**LALALAL**IAVIVVLLF**G**TKK*LGSIGSDLGASIKGFKKAMS*DDEP KQDKTSQDADFTAKTIADKQADTNQEQAKTEDAKRHDKEQV

The hydrophobic core of the TMH is indicated in bold (12 residues in *B. subtilis* as well as in *E. coli*), the interphase residues of the TMH are highlighted in gray bold and the residues of the APH are highlighted in italics. The mutations of the protein variants are underlined. Please note that the N-terminal methionine is cut off due to cyanogen bromide cleavage in case of the *B. subtilis* $TatA_{2\text{-}45}$ variants, which have been used for our structural analysis. However, the hydrophobic stretch of TatA is not affected by this cleavage, as the partly polar N-terminal part in front of the TMH is quite long.

temperatures of longer saturated phosphatidylcholine lipids would require unacceptably high temperatures during the measurements. Therefore, mono-unsaturated lipids (ω-9) were used to cover the range from DOPC (diC 18:1) to DNPC (diC 24:1). Within this series, the hydrophobic thickness of the bilayer ranges from 12.2 to 38.2 Å (calculated according to Marsh (56)). There are only few literature data available on the detailed hydrophobic thickness of the natural *B. subtilis* membrane or the inner bacterial membrane in general. The hydrophobic thickness of the *E. coli* inner membrane has been estimated using solid-state NMR to be around 27 Å (58). The average thickness of *E. coli* inner membrane proteins has been estimated to be 29.7 Å (59). Under the assumption that the general thickness of membrane proteins is adapted to the membrane thickness, any model membrane from DOPC (18:1, $d_c = 26.8$ Å) to DEiPC (20:1, $d_c = 30.6$ Å) would thus represent the natural situation. However, for our study, the natural situation is of less interest as we aim to monitor the protein under extreme conditions to understand its response. Our intention is to create a lipid environment, in which TatA can experience pronounced positive or negative hydrophobic mismatch (meaning that the TMH is longer or shorter than the hydrophobic thickness of the membrane, respectively).

For SRCD experiments in isotropic suspension, $TatA_{2\text{-}45}$ was reconstituted in small unilamellar lipid vesicles (SUVs). SRCD is a powerful tool for studying the secondary structure

TABLE 2 Lipids used in this study and their physical properties

Phosphatidylcholine lipids	Chain length	Abbreviation	T_m (°C)	d_c (Å)
1,2-Dioctanoyl-*sn*-glycero-3-phosphocholine	*di*C 8:0	DOcPC	–	12.2
1,2-Didecanoyl-*sn*-glycero-3-phosphocholine	*di*C 10:0	DDPC	–	16.6
1,2-Dilauroyl-*sn*-glycero-3-phosphocholine	*di*C 12:0	DLPC	−2	21.0
1,2-Dimyristoyl-*sn*-glycero-3-phosphatidylcholine	*di*C 14:0	DMPC	24	25.4
1,2-Dioleoyl-*sn*-glycero-3-phosphocholine	*di*C 18:1	DOPC	−17	26.8
1,2-Dieicosenoyl-*sn*-glycero-3-phosphocholine	*di*C 20:1	DEiPC	−4	30.6
1,2-Dierucoyl-*sn*-glycero-3-phosphocholine	*di*C 22:1	DErPC	13	34.4
1,2-Dinervonoyl-*sn*-glycero-3-phosphocholine	*di*C 24:1	DNPC	27	38.2
Phytanoyl lipids				
1,2-Diphytanoyl-*sn*-glycero-3-phosphocholine	*di*C 16:0(Me_4)	DPhPC	NA	27.2
1,2-Diphytanoyl-*sn*-glycero-3-phosphoethanolamine	*di*C 16:0(Me_4)	DPhPE	NA	

Lipid phase transition temperature (T_m) as reported by Avanti Polar Lipids (Alabaster, AL). The hydrophobic membrane thickness (d_c) at 30°C was calculated for saturated and unsaturated lipids according to Marsh (56), and for DPhPC it was derived from (57). Unsaturated chains are ω-9 and phytanoyl chains carry four methyl groups.

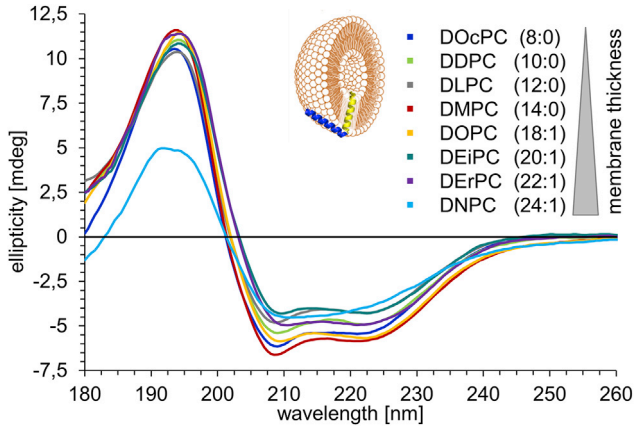

FIGURE 1 SRCD spectra of $TatA_{2\text{-}45}$ reconstituted in phosphatidylcholine lipid vesicles with varying membrane thickness. All SRCD spectra show a typical α-helical line shape with characteristic bands at 194, 209, and 223 nm. The spectrum of $TatA_{2\text{-}45}$ in DNPC shows an overall decrease in signal intensity, suggesting some degree of aggregation.

of biological macromolecules like membrane proteins. Compared with conventional CD spectroscopy, SRCD offers an extended wavelength range, a significantly better signal-to-noise ratio, and suffers far less from scattering artifacts (60,61). An additional advantage of SRCD is its applicability to systems containing unsaturated lipids, which cannot be measured in conventional CD, with a good signal-to-noise ratio at wavelengths below 200 nm due to the high background absorption of the lipid double bonds (52,61).

The SRCD spectra of $TatA_{2\text{-}45}$ in phosphatidylcholine vesicles with different membrane thickness show a positive band at 194 nm and two negative bands at 209 and 223 nm (see Fig. 1). The line shape suggests a predominantly α-helical secondary structure of $TatA_{2\text{-}45}$, irrespective of the bilayer thickness. Only in the exceptionally thick DNPC membranes, is a reduction of the signal intensity at 194 nm observed. This is a clear sign of absorption flattening (62), which can be attributed to an increasing degree of aggregation or clustering of $TatA_{2\text{-}45}$. Notably, all these spectra show the typical line shape of an α-helical protein, indicating that the membrane thickness has no effect on the actual folding or misfolding of $TatA_{2\text{-}45}$.

Influence of bilayer thickness on the membrane alignment of $TatA_{2\text{-}45}$

In a previous study, we examined the alignment of $TatA_{2\text{-}45}$ in DMPG/DMPC (70/30) bilayers in macroscopically oriented membranes using oriented CD (OCD). Those data revealed a surface-aligned orientation of the APH and a membrane-spanning orientation of the TMH (40), as expected from their respective amphiphilic/hydrophobic profiles. To determine the orientation of the two helical segments of the protein more accurately, the protein was labeled with ^{15}N and reconstituted in DMPC80/DMPG20/6-O-PC bicelles for 2D solid-state NMR analysis. In magnetically oriented bicelles, the transmembrane segment was found to be essentially "upright" with only a slight tilt angle of 13° relative to the bilayer normal, but the APH was considerably tilted by 64° instead of the anticipated 90° ("horizontal") alignment (32,41). These data suggested that the N-terminal end of the amphiphilic APH (which is connected to the TMH) is pulled quite deeply into the membrane by the unusually short TMH.

Here, we have extended these investigations to find out whether the membrane alignment of either of the two helical segments in $TatA_{2\text{-}45}$ is affected by bilayer thickness. Oriented solid-state ^{15}N-NMR and oriented synchrotron CD (SROCD) spectroscopy are complementary methods, ideally suited for monitoring the alignment of membrane proteins in macroscopically oriented lipid bilayers. They can provide the membrane alignment of α-helices, and routinely reveal any loss of alignment due to protein aggregation and/or unfolding (40,52,63–68). We thus reconstituted $TatA_{2\text{-}45}$ in oriented samples of the same lipid series as used above for the isotropic SRCD experiments. The quality of the phospholipid alignment was assessed from ^{31}P-NMR spectra collected before and after each ^{15}N-NMR experiment (see Fig. S2). All NMR and OCD measurements were performed using the standard sample alignment, in which the bilayer normal is aligned parallel to the static magnetic field or, respectively, to the incident light beam.

Fig. 2 *A* shows the 1D ^{15}N-NMR spectra of uniformly ^{15}N-labeled $TatA_{2\text{-}45}$ in oriented phosphatidylcholine bilayers with different membrane thickness. In lipids ranging from DLPC (21.0 Å) to DEiPC (30.6 Å), the signals of $TatA_{2\text{-}45}$ are separated into two distinct spectral regions. Signals in the downfield range of 170–220 ppm (highlighted in *yellow*) typically originate from helical segments that are oriented more or less parallel to the magnetic field and therefore correspond to a genuine transmembrane alignment. On the other hand, signals in the upfield range of 80–130 ppm typically originate from helices that are oriented more or less perpendicular to the magnetic field and are thus aligned along the membrane surface. The sharp signal at around 32 ppm is characteristic of the more flexible N-terminus and any lysine side chains of a protein (69). Hence, our qualitative spectral analysis in Fig. 2 *A* confirms the expected membrane alignment of $TatA_{2\text{-}45}$ in this extended set of lipid bilayers, demonstrating a membrane-spanning TMH and a surface-aligned APH, in full agreement with the protein structure and alignment previously determined in anionic planar bicelles (32).

Interestingly, in very thin DOcPC and DDPC membranes, the signals of the TMH are shifted upfield, indicating that the TMH of $TatA_{2\text{-}45}$ becomes significantly slanted due to positive hydrophobic mismatch. The orientation of the APH cannot be deduced in detail from these spectra, unfortunately, because the spectral region of the APH signals

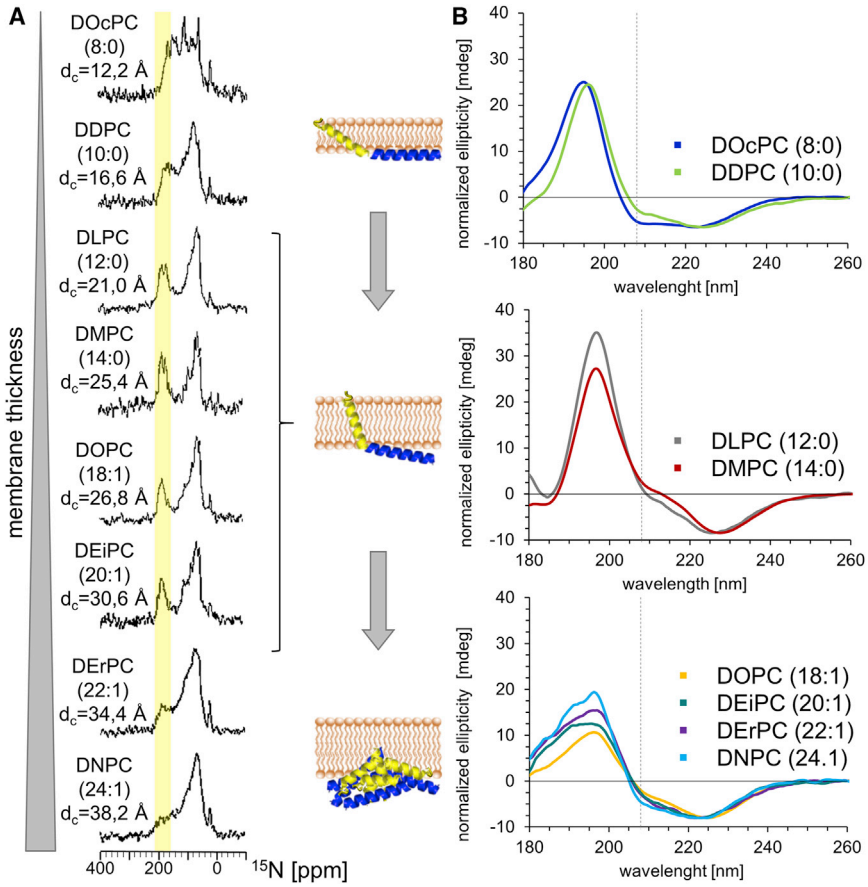

FIGURE 2 ^{15}N-NMR and SROCD spectra of $TatA_{2\text{-}45}$ reconstituted in macroscopically aligned phosphatidylcholine lipid bilayers with varying membrane thickness. (*A*) The ^{15}N-NMR spectra show that the TMH of $TatA_{2\text{-}45}$ has an almost upright orientation in the series from DLPC, DMPC, DOPC, and DEiPC, as reflected by distinct signal intensity in the range of 170–220 ppm (highlighted in *yellow*). With decreasing membrane thickness, these signals shift gradually upfield, indicating a more tilted alignment of the TMH. Pure powder spectra are observed in the case of DNPC and largely in DErPC, as a result of protein aggregation in these very thick bilayers. (*B*) According to the SROCD line shapes, the TMH of $TatA_{2\text{-}45}$ possesses an upright orientation in DLPC and DMPC. This is indicated by positive ellipticity values at 208 nm. A strong tilt of the TMH and a flat surface-aligned APH is observed in very short lipids (DOcPC and DDPC) with a strong negative signal at 208 nm. The increasing absorption flattening in DOPC to DNPC, together with an increase of the negative band at 208 nm, indicates aggregation of helical segments. In the SROCD samples, protein aggregation already seems to set in in somewhat thinner membranes than in ^{15}N-NMR samples. The global minima of the OCD spectra are scaled to the same intensity to allow comparing the different line shapes at the characteristic band around 208 nm (*dashed line*). A cartoon representation of $TatA_{2\text{-}45}$ visualizes the qualitative global orientation of the TMH in the membrane, as derived from our NMR/OCD spectra. The hydrophobic membrane thickness (d_c) is given for each lipid (see Table 2).

always contains some residual powder component due to slight sample heterogeneity (some amount of powder content is not surprising, as we monitor the protein under extreme conditions). In the case of the exceptionally short lipid DOcPC, an additional sharp isotropic signal at 120 ppm arises, originating from flexible protein components with high mobility, presumably as a result of partial unraveling of the helix. This observation shows that even the unusually short TMH of TatA with a hydrophobic length of 24 Å (see Table 3) is yet too long for these extremely thin bilayers with a hydrophobic thickness of only 12.2–16.6 Å (see Table 2). On the other hand, the membranes consisting of DErPC (34.4 Å) and DNPC (38.2 Å) are extremely thick, and we see that the spectrum of TatA has collapsed into a nonoriented powder line shape. Such powder pattern is composed of signals from all spatial orientations of the protein relative to the magnetic field, which indicates an overall loss of alignment. This lack of alignment can have many different reasons, such as unfolding and aggregation into β-sheets, or merely the clustering of α-helical segments into local domains with an extreme mosaic spread, or possibly the dissolution/fragmentation of the lipid bilayer into disordered patches, etc. Note that a ^{15}N-NMR powder spectrum alone does not reveal any information on the folded state of the protein, for which complementary SROCD experiments are required (the corresponding SROCD data will be discussed below). We note, nonetheless, that the TMH cannot span the bilayer any more in these extremely long-chain lipids, as it would be energetically unfavorable to pull the polar N-terminus and/or the

TABLE 3 $TatA_{2\text{-}45}$ variants and their physical properties

$TatA_{2\text{-}45}$ variants	Number of amino acids in the TMH	Sequence range of the TMH	TMH length (Å)	Number of helix turns	Variation
$TatA_{2\text{-}45}$ LALALAL	23	Pro_8–Pro_{30}	34.5	6.4	extension of the TMH
$TatA_{2\text{-}45}$ LALAL	21	Pro_8–Pro_{28}	31.5	5.8	extension of the TMH
$TatA_{2\text{-}45}$ LAL	19	Pro_8–Pro_{26}	28.5	5.3	extension of the TMH
$TatA_{2\text{-}45}$	16	Pro_8–Pro_{23}	24.0	4.4	natural TMH
$TatA_{2\text{-}45}$ ΔLIL	13	Pro_8–Pro_{20}	19.5	3.6	shortening of the TMH

The length of the TMH was calculated based on a 1.5 Å translation per residue, and 3.6 residues per helix turn.

amphiphilic helix any further into the hydrophobic membrane core. Such situation of pronounced hydrophobic mismatch between a monomeric protein and the surrounding lipid matrix is well known to lead to protein clustering and/or aggregation (70–73), as the line tension of the annular lipids gets relaxed that way.

Fig. 2 *B* shows the complementary SROCD data of $TatA_{2\text{-}45}$ reconstituted in the same lipid systems. In OCD, the "fingerprint" band around 208 nm gives information about the alignment of a helix in the bilayer. If the OCD band around 208 nm exhibits a strong negative intensity, a protein helix is aligned perpendicular to the incident light, and therefore parallel to the membrane surface. A decrease in the OCD signal around 208 nm toward zero implies a more tilted orientation of the protein helix. If the band around 208 nm shows zero or positive values, along with a shift of the positive band maximum from 193 to 196 nm, the alignment of the helix is parallel to the bilayer normal, which indicates a transmembrane inserted state (63,74). As CD spectroscopy only gives global information on secondary structure, OCD spectroscopy can only give global information on the orientation of the entire protein sequence used. When interpreting the spectra, one has to take into account that $TatA_{2\text{-}45}$ consists of a TMH plus an APH, and therefore the signals of both helices contribute to the OCD line shape. The SROCD spectra shown here have thus been normalized to facilitate the comparison of qualitative differences at the fingerprint band around 208 nm.

As already seen in the NMR data, the OCD spectra also show that the TMH of $TatA_{2\text{-}45}$ is strongly tilted in the thin lipids DOcPC and DDPC due to positive hydrophobic mismatch. Most probably the end of the APH does not get pulled into the membrane any more in these thin lipids and can reside flat on the membrane surface, which explains the very strong negative band around 208 nm. This band is even more pronounced in DOcPC than in DDPC, in good agreement with the NMR analysis, which already showed that the TMH is more strongly tilted in DOcPC. In bilayers with moderate thickness, as in DLPC and DMPC, the TMH appears to be aligned in a more or less upright state, suggesting that the hydrophobic stretch of the helix fits across the core of these bilayers (21.0–25.4 Å). The signal at 208 nm of the DMPC sample is even more positive than the one from DLPC, suggesting that the TMH is slightly more upright in DMPC bilayers (or the APH gets pulled inside the membrane to a greater degree). In thicker bilayers starting from DOPC up to DNPC, the negative intensity of the CD band around 208 nm increases again but remains less prominent than the band at 223 nm. Furthermore, strong absorption flattening below 200 nm is apparent, showing that the protein starts to cluster and/or aggregate. The increase of the negative band at 208 nm in these cases is most probably not due to a tilting of a helical segment. It can be explained by a loss of orientation due to the agglomeration of helical segments, which become unordered in the supposedly aligned sample (as seen above in the ^{15}N-NMR powder spectrum), such that the OCD spectrum then resembles the isotropic CD line shape of a helical segment. This observation provides the important piece of information that TatA aggregates without losing its α-helical conformation. On the side, we note that, in the OCD samples, this process starts already in DOPC (which fits to the expectations based on calculated bilayer thickness), whereas in NMR it becomes visible only in DErPC and DNPC bilayers, possibly due to slight differences in sample geometry and hydration.

In summary, both the solid-state ^{15}N-NMR and the SROCD data clearly demonstrate a structural adaption of $TatA_{2\text{-}45}$ to the membrane thickness. The TMH of $TatA_{2\text{-}45}$ aligns in an upright orientation in lipid bilayers only when the thickness is comparable with the hydrophobic length of the TMH segment. In thinner bilayers, the TMH responds to the hydrophobic mismatch by adjusting its tilt angle and by a relaxation of the membrane-pulled APH. Furthermore, in very thin bilayers some partial unraveling of the helix is visible. In thicker bilayers, the TMH of $TatA_{2\text{-}45}$ is obviously no longer able to span the membrane (even by pulling the end of the APH inside the bilayer), which leads to aggregation and/or clustering of the protein, as the polar N-terminus can no longer reach the polar surface. Interestingly, according to OCD, the aggregation/clustering is not accompanied by any unfolding of the helices.

Influence of TMH length on the membrane alignment of $TatA_{2\text{-}45}$

Having shown that the membrane alignment of $TatA_{2\text{-}45}$ depends on the external bilayer thickness, as a next step we examined the influence of the hydrophobic length of the transmembrane sequence itself. For this purpose, we produced $TatA_{2\text{-}45}$ variants with different hydrophobic TMH lengths (see Tables 1 and 3). One variant with a shortened TMH was created by deleting three hydrophobic amino acids: $Leu_{10}Ile_{11}Leu_{12}$ ($TatA_{2\text{-}45}$ ΔLIL). A further three variants with a successively elongated TMH were generated by inserting repeated leucine-alanine motifs into the transmembrane region ($TatA_{2\text{-}45}$ LAL, $TatA_{2\text{-}45}$ LALAL, $TatA_{2\text{-}45}$ LALALAL). The corresponding TMH lengths of all four variants range from 19.5 to 34.5 Å (see Table 3).

SRCD analyses of these variants demonstrate that the overall α-helical folding is not influenced by the mutations (see Fig. S3). To determine their membrane alignment, we reconstituted the variants in macroscopically oriented lipid bilayers composed of DMPC (with a hydrophobic thickness of 25.4 Å that is well suited to accommodate the wild-type protein) and investigated the samples as above using SROCD and ^{15}N-NMR (see Fig. 3). The ^{15}N-NMR spectra show that the signals of the TMH (highlighted in *yellow*)

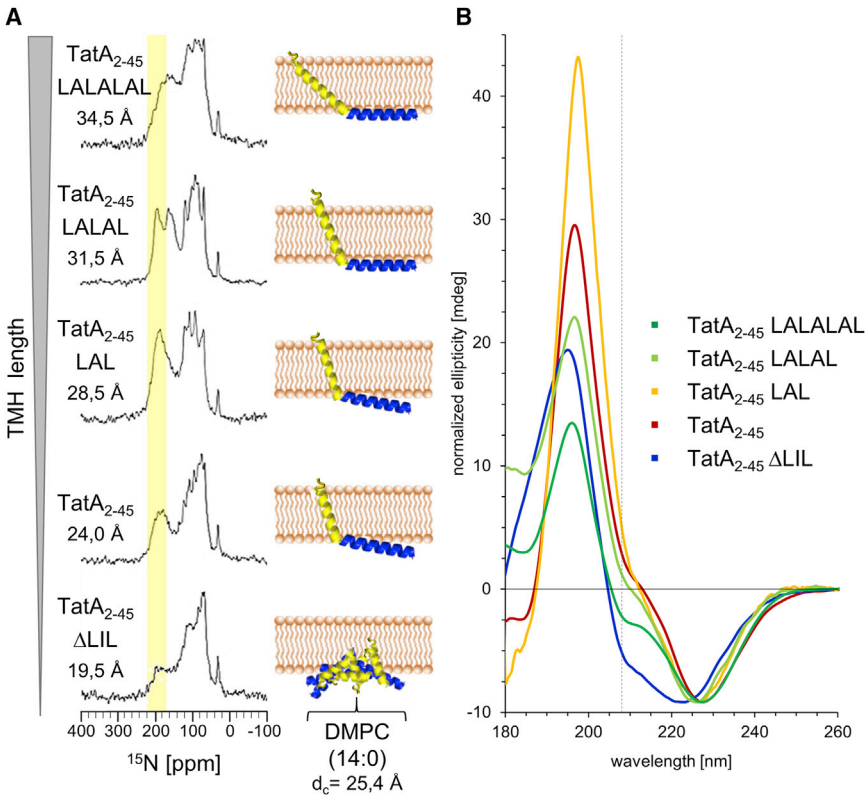

FIGURE 3 ^{15}N-NMR and SROCD spectra of $TatA_{2\text{-}45}$ variants with an extended or shortened TMH reconstituted in macroscopically aligned lipid bilayers composed of DMPC. (*A*) The signals of the TMH (highlighted in *yellow*) gradually shift upfield with increasing TMH length, indicating that the TMHs of the variants with an extended TMH become tilted more and more due to the hydrophobic mismatch. The shortened $TatA_{2\text{-}45}$ ΔLIL shows a high powder content, indicating protein aggregation, because the TMH is too short to span the lipid bilayer. (*B*) Within the series of the SROCD spectra, the negative band at 208 nm increases with increasing TMH length, indicating a more tilted TMH alignment of the $TatA_{2\text{-}45}$ variants with an extended TMH (and also the APHs become less and less pulled into the membrane in these variants). A reduction of the signal intensity at around 196 nm is also observed with increasing TMH length (starting from TatA LALAL), indicating some amount of protein aggregation. The $TatA_{2\text{-}45}$ ΔLIL mutant seems to aggregate, but retains its helical orientation, indicated by a strong reduction in the signal intensity around 194 nm together with a pronounced band at 208 nm. The global minima of the spectra are scaled to the same intensity to allow comparison of the different line shapes at the characteristic band at 208 nm (*dashed line*). A cartoon representation of $TatA_{2\text{-}45}$ visualizes the qualitative global orientation of the TMH in the membrane, as derived from our NMR/OCD spectra. The calculated TMH length for each $TatA_{2\text{-}45}$ variant (see Table 3) and the hydrophobic membrane thickness (d_c) of DMPC lipid bilayers (see Table 2) are given.

shift upfield with increasing TMH length of the $TatA_{2\text{-}45}$ variants, indicating that the extended helixes become more and more slanted (see Fig. 3 *A*). One might expect the APH to reside flat on the membrane surface under these relaxed conditions without negative hydrophobic mismatch; however, this cannot be directly derived from the NMR spectra due the overlay of residual powder pattern signals. Just as was the case for $TatA_{2\text{-}45}$ in very thin membranes, these variants compensate the positive hydrophobic mismatch by increasing the tilt angle of the TMH to prevent an exposure of hydrophobic side chains to the hydrophilic environment. On the other hand, mutant $TatA_{2\text{-}45}$ ΔLIL with a shortened TMH shows a significant contribution of a nonoriented signal in the ^{15}N-NMR spectrum. This observation suggests that protein aggregation/clustering occurs under equivalent mismatch conditions, determined by the ratio of helix length to bilayer thickness, as observed above for $TatA_{2\text{-}45}$ in thick DErPC and DNPC membranes. For purely physical reasons, any TMH that is too short to span the bilayer will assemble laterally into clusters and eventually aggregate and leave the lamellar lipid matrix. When TatA can no longer pull its polar N-terminus and/or the connected amphiphilic helix any more deeply into the hydrophobic membrane core, the TMH will respond accordingly.

Within the SROCD series of the elongated TatA variants, the negative band at around 208 nm becomes gradually more and more negative from $TatA_{2\text{-}45}$ LAL to $TatA_{2\text{-}45}$ LALALAL (see Fig. 3 *B*). This observation suggests that the TMH becomes progressively slanted with increasing length (while the APH is pulled into the membrane less and less), which is in full agreement with the solid-state NMR data described above. At the same time, some absorption flattening at wavelengths below 200 nm is observed with increasing TMH length (starting from $TatA_{2\text{-}45}$ LALAL), indicating protein aggregation/clustering. The deletion of only three amino acids ($TatA_{2\text{-}45}$ ΔLIL) leads to a strong negative band at around 208 nm. This mutant shows also considerable absorption flattening at lower wavelengths. The OCD data thus suggest that $TatA_{2\text{-}45}$ ΔLIL tends to aggregate/cluster in DMPC, while retaining its helical conformation, which would explain the negative band at 208 nm.

In summary, the hydrophobic length of the transmembrane segment influences the orientation of the TMH in the same way as the bilayer thickness does. Positive hydrophobic mismatch leads to an increased slant of the TMH (and less membrane-immersed APH), whereas negative hydrophobic mismatch leads to considerable aggregation and/or clustering without any unfolding of the helices.

Influence of the N-terminal charge of $TatA_{2\text{-}45}$ on the membrane alignment

As discussed above, the polar N-terminus of $TatA_{2\text{-}45}$ might explain the observed aggregation under negative hydrophobic mismatch conditions. The N-terminal amino group of a protein typically has a pK_a value of about 7.7 (75). Having used the organic solvent 1,1,1,3,3,3-hexafluoro-2-propanol (HFIP) for reconstitution of $TatA_{2\text{-}45}$, the pH value of our NMR and CD samples is slightly acidic (pH 5–6), so we can expect the N-terminus of $TatA_{2\text{-}45}$ to be predominantly protonated in the oriented membrane samples. Such a charged N-terminus will reside on the hydrophilic face of the membrane if the TMH spans the lipid bilayer completely. It would be energetically unfavorable to pull this charge and the adjacent polar residues (Ser, Asn) deeper into the hydrophobic membrane core. When the membrane was too thick in the experiments above, as a consequence we observed an expulsion of the TMH, resulting in aggregation/clustering of the entire protein. To clarify this effect, we wondered whether an increased N-terminal charge would influence the membrane alignment and aggregation tendency of $TatA_{2\text{-}45}$. $TatA_{2\text{-}45}$ was thus mutated further to carry either one or two additional charges near the N-terminus (see Table 1). Aspartic acid was substituted for Phe_2 ($TatA_{2\text{-}45}$ F_2D), and for both Phe_2 and Ile_7 ($TatA_{2\text{-}45}$ F_2 D I_7D) in the *B. subtilis* sequence. We chose the negatively charged aspartic acid to minimize the influence on the total charge of the TMH (total charge of the TMH under slightly acidic conditions: wt = +1; $TatA_{2\text{-}45}$ F_2D = 0; $TatA_{2\text{-}45}$ F_2 DI_7D = −1). Furthermore, the short side chain of Asp prevents any snorkelling toward the bilayer surface. SRCD analysis of these charged variants reconstituted in vesicles prepared from long-chain lipids (DOPC, DEiPC, and DErPC) proved that the mutations did not influence the overall α-helical folding of the protein (see Fig. S4). However, in DEiPC vesicles, some absorption flattening is apparent, which is even more pronounced in DErPC. This can be attributed to an increased tendency toward aggregation/clustering of the charged variants compared with the wild-type. To determine the membrane alignment in detail, we used solid-state ^{15}N-NMR (in this case no SROCD was done, because the data in Fig. 2 showed that, under these conditions, aggregation of $TatA_{2\text{-}45}$ already started in DOPC).

The ^{15}N-NMR spectra show that aggregation of the increasingly polar variants starts in successively thinner membranes (see Fig. 4). In DOPC and DEiPC, $TatA_{2\text{-}45}$ still shows reasonably resolved spectra, suggesting an almost upright membrane-spanning orientation of the TMH (highlighted in *yellow*) without aggregation. In contrast, the single exchange mutant $TatA_{2\text{-}45}$ F_2D elicits a significant powder contribution in DEiPC, and the double exchange

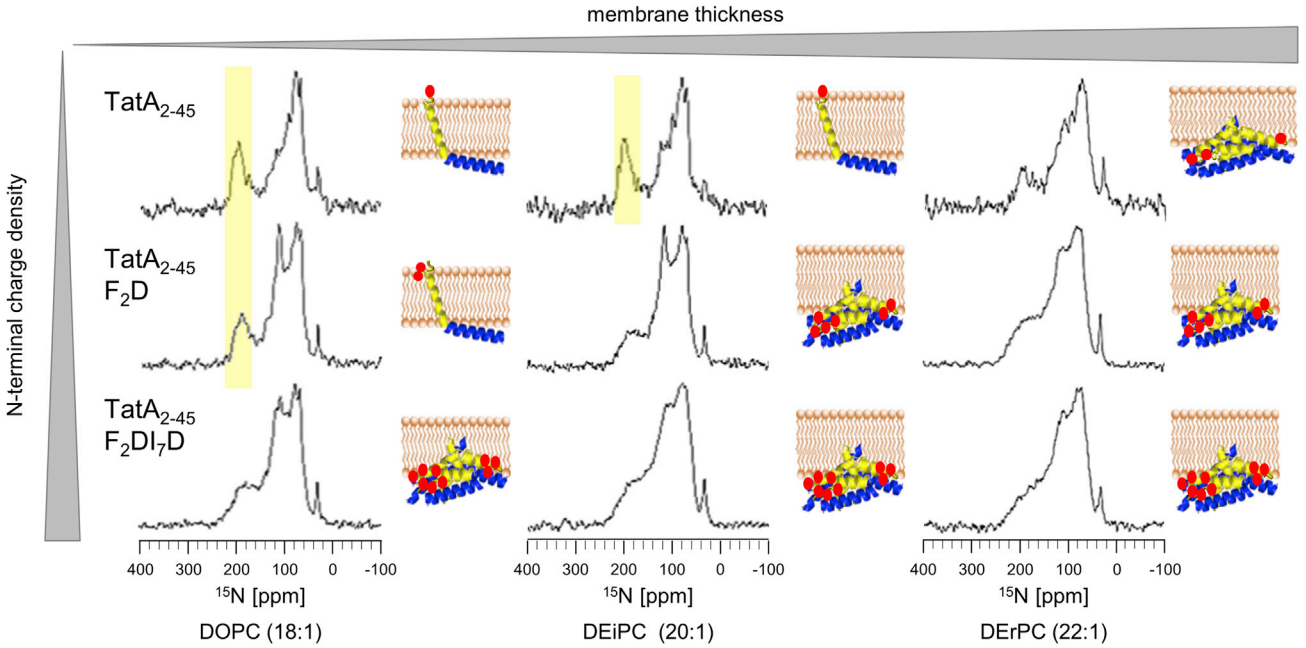

FIGURE 4 ^{15}N-NMR and SROCD spectra of $TatA_{2\text{-}45}$ variants with varying N-terminal charge density, reconstituted in macroscopically aligned lipid bilayers composed of DOPC, DEiPC, and DErPC. Inspection of the ^{15}N-NMR spectra shows that the introduction of charged amino acids near the N-terminus leads to an increased tendency of protein aggregation, which sets in already in thinner membranes. In DOPC membranes $TatA_{2\text{-}45}$ and $TatA_{2\text{-}45}$ F2D are still well oriented, whereas $TatA_{2\text{-}45}$ F2DI7D is already aggregated. In the longer DEiPC membranes, only $TatA_{2\text{-}45}$ is still oriented (highlighted in *yellow*) and, in the even longer DErPC membranes, all proteins aggregate. A cartoon representation of $TatA_{2\text{-}45}$ visualizes the qualitative global orientation of the TMH in the membrane, as derived from our NMR spectra (*red dots* represent the charged N-terminus or the aspartate mutations). To see this figure in color, go online.

mutant $TatA_{2\text{-}45}$ F_2DI_7D starts to aggregate/cluster already in DOPC. ^{31}P-NMR spectra of the lipids in the presence of the charged TatA variants, too, show a considerably high powder contribution, indicating a perturbation of the bilayer alignment due to their inability to accommodate the additional charges on the protein (see Fig. S2).

In summary, these data indicate that the polar N-terminus is responsible for the aggregation behavior observed under negative hydrophobic mismatch conditions, at least under ambient or slightly acidic pH. A stable membrane-anchored orientation of the TMH is no longer possible when the polar N-terminus or any additional charged amino acid would have be to become embedded too deeply within the hydrophobic membrane environment.

Influence of spontaneous bilayer curvature on the membrane alignment of $TatA_{2\text{-}45}$

When the TMH was too short to span the membrane, we observed protein aggregation and/or clustering in the NMR and CD experiments described above. However, it is important to realize that—even though the proteins and lipid molecules lost their alignment in the oriented NMR samples—the α-helical conformation of $TatA_{2\text{-}45}$ and its variants was nevertheless maintained, as indicated by the characteristic OCD line shapes. This finding implies that the short TMH of the protein gets expelled from the membrane core as a response to the hydrophobic mismatch, while remaining properly folded. Its only option now is to be accommodated near the bilayer surface, allowing both the polar N-terminus and the APH to reach the hydrophilic environment on the same face of the membrane. Under the conditions used so far, this process was accompanied by lateral clustering of the proteins and a loss of their preferred orientation, presumably because the protein concentration was too high and perturbed the lipid packing. To find out whether a stable surface-aligned orientation of the entire $TatA_{2\text{-}45}$ molecule (i.e., both the TMH and the APH) is feasible at all, we thus needed to change the sample conditions. Reducing the protein concentration is problematic in solid-state NMR due to the intrinsically limited sensitivity of this method. However, a lipid with a highly negative spontaneous curvature would be able to accommodate the expelled $TatA_{2\text{-}45}$ molecules more favorably in the surface region between the headgroups, at least in terms of the spatial requirements. We therefore reconstituted the protein in macroscopically aligned bilayers composed of the branched-chain lipid DPhPC (1,2-diphytanoyl-sn-glycero-3-phosphocholine; di-C 16:0, 3*me*, 7*me*, 11*me*, 15*me*) (57). Phytanoyl lipids possess a highly negative spontaneous curvature due to their branched acyl chains, while still forming stable bilayers. Earlier studies on antimicrobial peptides have demonstrated that the lipid shape, i.e., the spontaneous lipid curvature, has a dramatic influence on the membrane alignment of amphiphilic helices (76–82). Lipids with a high negative spontaneous curvature (higher lateral pressure in the acyl chain region than in the choline headgroup region) prevent insertion of these peptides into the membrane. Lipids with a high positive spontaneous curvature (large headgroup volume compared with acyl chains, leading to a higher lateral pressure in the headgroup region than in the hydrophobic core), on the other hand, allow their tilting and full insertion (as oligomers) across the hydrophobic core. The same effect was reported for the folding and insertion of β-barrel outer membrane proteins from bacteria (83).

Phytanoyl lipids should thus promote an expulsion of the transmembrane-anchored $TatA_{2\text{-}45}$ out of the membrane core and into the headgroup region. Because of the comparatively low packing density of the DPhPC headgroup region compared with the unbranched phosphatidylcholine bilayers used above, we would expect that there is enough space in DPhPC to accommodate the entire TatA molecule near the headgroup region. In that case the protein may not need to aggregate/cluster but could still remain monomeric and well oriented, embedded in a stable bilayer environment. This scenario should lead to an alignment of the entire $TatA_{2\text{-}45}$ protein more or less parallel to the membrane surface, i.e., of both TMH and APH. To facilitate this effect further, we used a lipid mixture containing, in addition, some DPhPE, because the small ethanolamine headgroup of DPhPE provides even more space in the headgroup region. Since the addition of DPhPE bears the risk of promoting the formation of hexagonal phases, we used only 5% DPhPE in our experiments and checked the lipid alignment before and after every ^{15}N-NMR measurement using ^{31}P-NMR (see Fig. S2). In this respect it also important to note that DPhPC, despite having negative spontaneous curvature, is known to maintain the stable lamellar phase over a large temperature range (84). This allowed us to measure these samples at a moderate temperature of 22°C to avoid drying of the sample, as dehydration would enhance the risk of forming non-lamellar phases (85). The corresponding SRCD analysis of $TatA_{2\text{-}45}$ and its variants reconstituted in DPhPC/DPhPE (95/5 mol/mol) vesicles prove that the proteins retain their overall α-helical folding. The variants with an extended TMH show an increased helicity compared with $TatA_{2\text{-}45}$, as expected due the increased length, whereas the destabilized $TatA_{2\text{-}45}$ ΔLIL variant shows some degree of β-stranded signal, presumably due to partial unfolding (see Fig. S5).

The ^{15}N-NMR spectra (see Fig. 5 *A*) of the variants with an extended helix ($TatA_{2\text{-}45}$ LAL, LALAL, and LALALAL) show that the TMH is properly inserted upright in phytanoyl membranes. These variants possess a transmembrane segment that is long enough to span the lipid bilayer completely, allowing the charged N-terminus to reach the hydrophilic surface (see Tables 2 and 3). For wild-type $TatA_{2\text{-}45}$ with its native TMH, however, the situation is different. In this very important case, the signal intensity of the TMH in the upright state is clearly reduced in the ^{15}N-NMR spectrum. We see that most

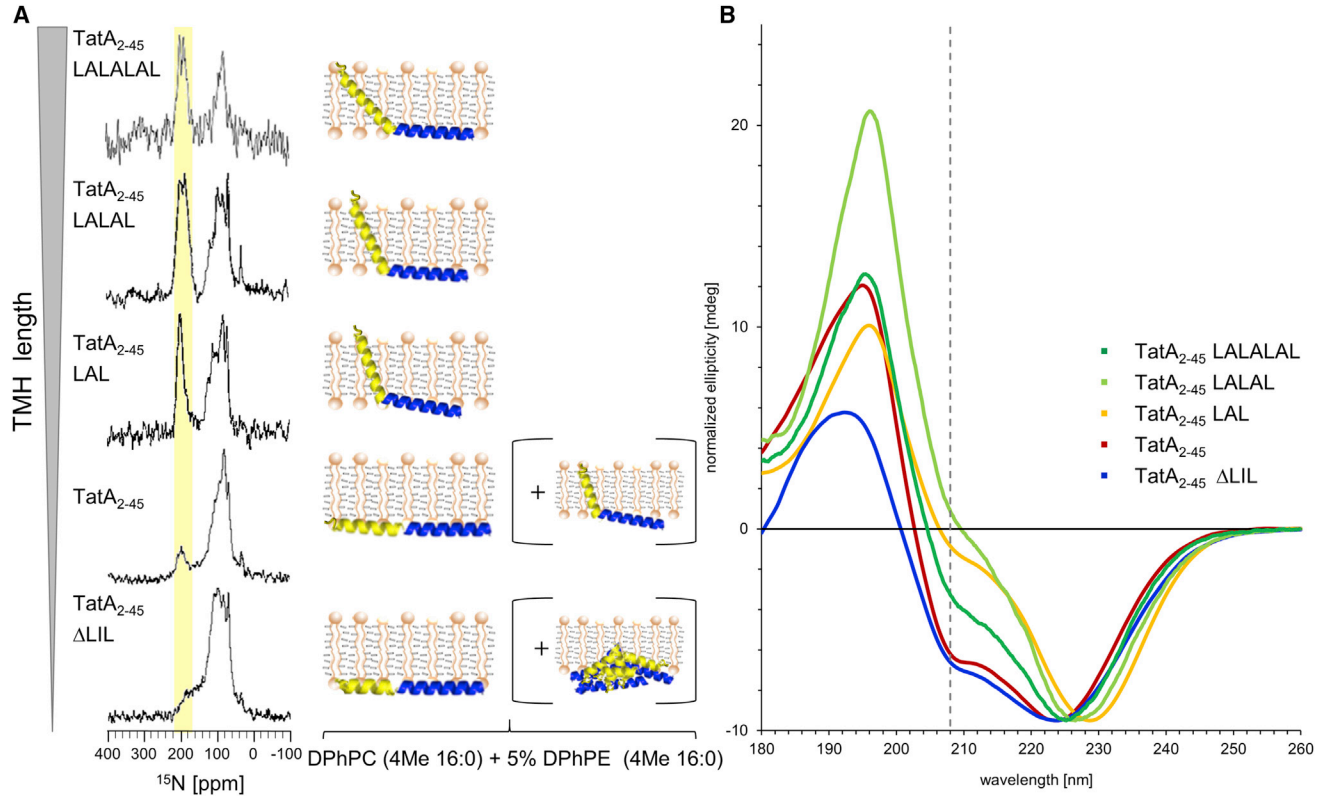

FIGURE 5 ^{15}N-NMR and SROCD spectra of $TatA_{2\text{-}45}$ reconstituted in oriented lipid bilayers composed of phytanoyl lipids with a highly negative spontaneous curvature. (*A*) The ^{15}N-NMR spectra show that phytanoyl lipids support a transmembrane inserted state of the TMH only for the variants with an extended TMH ($TatA_{2\text{-}45}$ LAL, $TatA_{2\text{-}45}$ LALAL, and $TatA_{2\text{-}45}$ LALALAL). The wild-type $TatA_{2\text{-}45}$ shows a reduced signal of the TMH, suggesting that it flips at least partially out of the membrane core. The mutant $TatA_{2\text{-}45}$ ΔLIL with a shortened TMH gives no signal of the TMH anymore, but an underlying powder pattern becomes visible. (*B*) SROCD shows that the TMH of the variants $TatA_{2\text{-}45}$ LAL and $TatA_{2\text{-}45}$ LALAL assume a transmembrane inserted state. The mutant $TatA_{2\text{-}45}$ LALALAL exhibits an increasing negative band at 208 nm, indicating a tilted orientation of the TMH due to positive hydrophobic mismatch (and a flatter surface-aligned APH). The wild-type TMH, as well as the shortened TMH in $TatA_{2\text{-}45}$ ΔLIL, seem to flip onto the membrane surface, as indicated by the strong negative band at 208 nm. The $TatA_{2\text{-}45}$ ΔLIL mutant not only flips onto the membrane surface, but partly also aggregates there, as indicated by some amount of absorption flattening. A cartoon representation of $TatA_{2\text{-}45}$ visualizes the qualitative global orientation of the TMH in the membrane, as derived from our NMR/OCD spectra.

of the TMH segments have "flipped" out of the membrane (strong reduction in the characteristic "transmembrane" NMR signal around 200 ppm) and ended up parallel to the membrane surface. The term "flip" is used to describe the reorientation between the two stable states seen in different lipid systems (but it should not imply that the TMH is continually flipping back and forth between these two states). Obviously, it is no longer energetically favorable for the TMH to span the bilayer in phytanoyl lipids, so now the entire $TatA_{2\text{-}45}$ molecule becomes aligned parallel to the membrane surface in a well-ordered manner. The other lipid systems used above had always shown significantly increased contribution from nonoriented protein content under conditions of negative hydrophobic mismatch. In DPhPC (with 5% DPhPE); however, there is no such contribution, as the ^{15}N-NMR spectrum consists only of two discrete signals, with no underlying broad powder component. Also, the ^{31}P-NMR spectra demonstrate that the DPhPC/DPhPE (95/5 mol/mol) matrix remains intact as a well-aligned lamellar bilayer (see Fig. S2). Therefore, it seems that our idea of providing more space in the headgroup region for the expelled TMH was successful and indeed supports a flipping of the TMH while at the same time preventing aggregation/clustering.

At this point, it is important to note that, if we regard only the hydrophobic bilayer thickness per se, $TatA_{2\text{-}45}$ should be able to span a DPhPC bilayer (27.2 Å) and compensate for a moderate hydrophobic mismatch. That is because DOPC (26.8 Å) and even DEiPC (30.6 Å) have comparable thickness, and in those lipids the TMH was found to be upright and well oriented in the NMR spectra (see Fig. 2 *A*). The data in DPhPC therefore highlight several factors that contribute to the balance between the transmembrane and surface-aligned state of the TMH: 1) the geometrical (and implicitly thermodynamic) argument of hydrophobic mismatch obviously drives the increased tilt (bilayer too thin) and the flip (bilayer too thick) of the TMH; 2) the lipid shape, too, plays an important role in optimizing lipid-lipid and lipid-protein interactions, favoring either a transmembrane (cylindrical lipid shape) or a surface-alignment (conical lipid shape with a negative curvature, i.e., small headgroup or voluminous chains). On top of

that, 3) not only do the relative dimensions of the helix length and bilayer thickness needed to be considered, but also the absolute hydrophobicity of the TMH. That is, a shortened hydrophobic helix is anchored less tightly in the membrane core due to decreased van der Waals interactions with the lipid acyl chains. Accordingly, the mutant $TatA_{2\text{-}45}$ ΔLIL with a shortened TMH shows nearly no transmembrane NMR signal anymore. In this case, all molecules have flipped out of the membrane completely, giving rise to a combination of well-ordered surface-bound protein, as well as some aggregated/clustered material.

The analogous SROCD analysis confirms these results (see Fig. 5 *B*). The TMH lengths of the variants $TatA_{2\text{-}45}$ LAL (28.5 Å) and $TatA_{2\text{-}45}$ LALAL (31.5 Å) match the hydrophobic membrane thickness of the DPhPC bilayer (27.2 Å) quite well (see Tables 2 and 3). Indeed, these variants are found to span the lipid bilayer in an essentially upright state according to the positive (or in the case of $TatA_{2\text{-}45}$ LAL only weakly negative, which might reflect a bit less tight anchoring in the membrane) band at 208 nm. At first sight the mutant $TatA_{2\text{-}45}$ LALALAL seems to lie out of order, as it shows an increase of the negative band at 208 nm. However, this cannot be contributed to by a flipping of the TMH, as we know from the NMR data, but instead reflects a tilting of the extended TMH due to positive hydrophobic mismatch (and a flatter surface-aligned APH). This example illustrates once more why it is so important to use a combination of oriented NMR and OCD as complementary techniques, as the information available from either method alone would remain ambiguous or incomplete. The important point in Fig. 5 *B* is that the OCD data of $TatA_{2\text{-}45}$ wild-type and $TatA_{2\text{-}45}$ ΔLIL show a strong negative band at 208 nm, indicating that the TMH has flipped out of the membrane core again, fully supporting the ^{15}N-NMR results above. For $TatA_{2\text{-}45}$ ΔLIL, some absorption flattening is visible, which can be attributed to some nonoriented protein content, as has been also noted from the NMR data.

In summary, these NMR and OCD results provide solid evidence that the entire $TatA_{2\text{-}45}$ protein (i.e., both TMH and APH) can be aligned parallel to the membrane surface in a stable manner while maintaining its α-helical conformation. We thus conclude that the TMH of $TatA_{2\text{-}45}$ has a length that is sufficient, on the one hand, to anchor the protein in the membrane, just like any other conventional hydrophobic transmembrane segment. However, at the same time, the unusually short length of the TMH provides $TatA_{2\text{-}45}$ with an intrinsic ability to flip out of the membrane under special conditions and reside on the bilayer surface in an essentially horizontal alignment. In our biophysical model membranes, we triggered this unusual flipping of the transmembrane helix simply by adjusting the parameters of hydrophobic mismatch and negative lipid curvature.

Monte Carlo simulations for characterization of the surface-aligned TMH

So far, we have demonstrated that both TMH and APH can be aligned parallel to the membrane surface in a stable manner, but neither NMR nor OCD has given any information on how deeply either segment is embedded within the polar/amphiphilic region of the lipid bilayer. This aspect can be addressed using all-atom Monte Carlo (MC) simulations of TatA, which will also provide a more detailed picture of the surface-aligned state altogether. Since the polarity and charge of the N-terminus were found to affect the flipping of the TMH (see Fig. 4), we decided to also analyze and compare the effect of its protonation state (given that the N-terminal pK_a value of a protein is typically around 7.7 (75)). $TatA_{1\text{-}45}$ was embedded in an implicit membrane model with a hydrophobic thickness of 42 Å, which is much too thick to allow the N-terminus to reach across to the opposite side. The first MC run in Fig. 6 *A* shows that the membrane-inserted TMH with a deprotonated N-terminus remains stable in the hydrophobic core of the bilayer throughout the entire simulation. However, when it is protonated, the TMH gets flipped out during the simulation and ends up lying parallel to the membrane surface (see Fig. 6 *B* and Video S1), as was seen in the slightly acidic NMR and OCD samples.

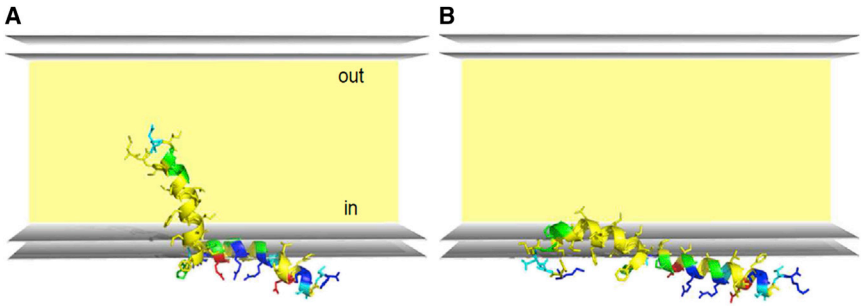

FIGURE 6 MC simulation of $TatA_{1\text{-}45}$ with a deprotonated and protonated N-terminus in an implicit membrane model. Snapshot of all-atom MC simulations of $TatA_{1\text{-}45}$ in an implicit membrane model with a hydrophobic bilayer thickness of 42 Å to examine the role of the N-terminal protonation state and to reveal the structure of the surface-aligned TMH. (*A*) The deprotonated TMH is stably inserted inside the membrane during the whole simulation. (*B*) When protonated, the N-terminal helix flips toward the membrane surface and remains there adopting a "banana-shaped" structure, which is kinked in a way that the charged N-terminus and the polar residues point into the hydrophilic environment (see Video S1). To see this figure in color, go online.

Several new insights can be derived from the MC analysis. First, the flipped protonated TMH is embedded near the upper edge of the hydrophobic bilayer core, i.e. more deeply than the amphiphilic APH, which resides in the polar headgroup layer, as expected. Interestingly, the TMH adopts a "banana-shaped" structure in this interphase region, without any discernible breaking of the helix, keeping its two polar ends closer to the hydrophilic layer. The curved helical structure seems to be stabilized by π-π stacking interactions (86) and/or hydrophobic packing of the three Phe residues that are lined up on the same face of the TMH at the beginning, middle, and end of the helix. This orientation allows the hydrophobic residues to remain immersed within the upper acyl chain region of the membrane, while the charged N-terminus and other polar residues are oriented toward the hydrophilic environment. The immersion of the hydrophobic residues in the upper acyl chain region of the membrane keeps the TMH adsorbed to the surface of the membrane. The MC simulations thus confirm that the protonated/charged N-terminus inside a hydrophobic environment is indeed the driving force for the experimentally observed flipping of the TMH and, in addition, the simulation provides a first impression on the depth and rotational alignment of the surface-aligned TMH.

In vitro translocation assay demonstrating the functional relevance of the short TMH of TatA

The structural investigations of $TatA_{2\text{-}45}$ in model membranes have highlighted an interesting ability of this unusually short TMH to flip between two alignment states, as it can exist not only in a genuine transmembrane bound state but also in a stable surface-aligned state. To examine the functional relevance of this unusual property of the short TMH, we performed an in vitro translocation assay in *E. coli* (87). The wild-type TatA was compared with variants carrying an extended TMH, which should experience a stronger anchoring in the bacterial membrane. We monitored the transport of the natural *E. coli* Tat substrate AmiC into inverted inner membrane vesicles (INVs) upon synthesis via in vitro transcription/translation. Externally added proteinase K (PK) digests AmiC completely when there are no INVs present (see Fig. 7 *B*: INV–). However, in the presence of INVs prepared from a TatABCD overproducing *E. coli* strain (*E. coli* BL21 [DE3] ΔTat complemented with plasmid pET22b + TatABCD), a significant amount of AmiC is seen to become resistant to PK treatment because it was transported into the lumen of the vesicles by the functional Tat translocase (see Fig. 7 *B*: TatA wt). An additional proof for successful translocation is the appearance of the mature form of AmiC (on the SDS-PAGE) due to cleavage by the signal peptidase. This band is generally accompanied by a certain amount of AmiC precursor protein that appears resistant to PK treatment, because it is known that the cleavage of the signal peptide is not strictly coupled to translocation in this in vitro experiment (30,87). We produced a series of three TatA variants (extended by LAL, LALA, and LALALAL) and verified the presence of all translocase components (TatA, TatB, and TatC) by western blotting with the corresponding antibodies (see Fig. 7 *A*). By comparison of the synthesized amount of AmiC with the amount that has been transported into the lumen, we quantified the transport efficiency (TE) on the basis of three independent experiments. Our assay shows that the transport of AmiC into INVs gets successively reduced when the hydrophobic stretch of the TMH is being elongated (see Fig. 7 *B*). The TatA wild-type shows considerable transport into the vesicles (TE = 35%), but already the transport rate of the LAL variants is reduced by half (TE = 16%), and the TatA variants with even longer TMHs (LALA and LALALAL) have abolished transport almost completely (TE = 3 and 1%, respectively). Notably, the TatA LAL variant displays essentially the same helix orientation as the TatA wild-type protein in DMPC membranes (as seen in Fig. 3). However, its elongated hydrophobic segment seems to anchor the protein more tightly in the membrane (see Fig. 5) due to enhanced van der Waals interactions. Therefore, the reduced activity can be attributed to the tighter anchoring of the longer hydrophobic stretch in the membrane, rather than to an inability of the longer TMH of TatA to functionally interact with TatC due to any significant change in orientation. This assay thus proves that the unusually short length TMH of TatA is critically required for proper functioning of the TatA translocation machinery.

DISCUSSION

The $TatA_d$ protein, with a length of 70 amino acids, represents one of the two key components of the minimal Tat translocase in *B. subtilis* (12–14). It is assumed that TatA permeabilizes the membrane, while TatC, the second key component of the Tat translocase, recognizes the cargo and initiates the translocation process (8). However, the detailed functional mechanism of this ΔpH-driven translocation machinery has remained elusive so far. Circular dichroism and solid-state NMR spectroscopy have been previously used to verify the predicted membrane alignment of $TatA_d$, consisting of an N-terminal transmembrane helix (TMH), an amphiphilic helix (APH) that lies at an oblique angle on the membrane surface, and an unstructured C-terminal region (32,40,41). Notably, the TMH is composed of only 12–16 amino acids (12 hydrophobic amino acids plus flanking Pro and Gly residues on both sides) (32), so it has a length of only 18–24 Å. This is much shorter than the typical stretch of 20–24 hydrophobic amino acids that is commonly found for single-span integral membrane proteins (88–90). It is well known that hydrophobic mismatch can lead to different responses of helical segments, such as helix tilting, conformational changes,

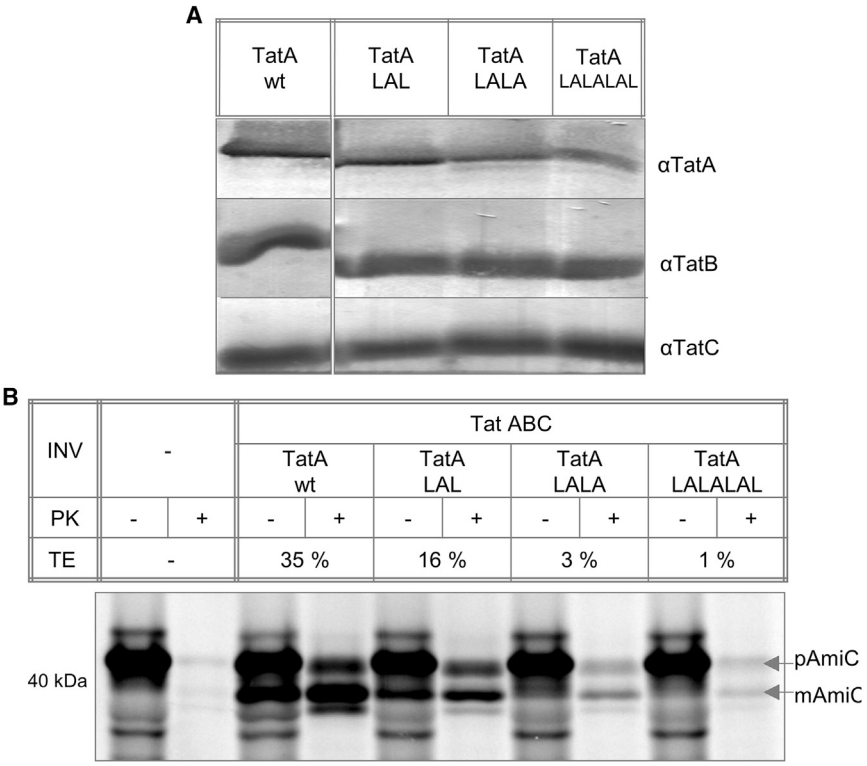

FIGURE 7 In vitro translocation assay of TatA variants with an extended TMH. (*A*) The presence of TatA, TatB, and TatC in the INVs is monitored using western blots with the corresponding antibodies. In all INVs sufficient amounts of the Tat components were present. However, the expression rate of the TatA variants with a massively extended TMH was slightly reduced. (*B*) The transport of the natural *E. coli* Tat substrate AmiC into INVs was monitored. Radioactively labeled AmiC was synthesized by means of in vitro transcription/translation in the presence or absence of INVs. After PK treatment to digest all untransported substrate, only AmiC that has been transported into the lumen of the INVs is detectable in the subsequent SDS-PAGE analysis. A transport efficiency (TE) was quantified on the basis of three independent experiments by comparison of the synthesized amount of AmiC with the amount that has been transported into the lumen. INVs containing the wild-type Tat components (TatA wt) show considerable transport into the vesicles (TE = 35%). It is seen that the transport efficiency is gradually reduced with increasing TMH length (TatA LAL = 16%; TatA LALA = 3%; TatA LALALAL = 1%). This observation proves that the unusually short length of the TMH of TatA plays an important role in the translocation process.

aggregation, or even reorientation (52,58,65,72,73,78,91–94). Therefore, we examined the membrane alignment of the unusually short TMH of TatA in model membranes under the influence of hydrophobic mismatch and spontaneous bilayer curvature.

SRCD analysis confirmed that the α-helical secondary structure of $TatA_{2\text{-}45}$ and its variants is preserved irrespective of membrane thickness and spontaneous curvature (see Figs. 1 and S3–S5). These data are in full agreement with our previous CD studies that had revealed a predominately α-helical conformation of $TatA_d$ in different membrane-mimicking environments (40). Our current findings are also in full accordance with CD experiments on *E. coli* TatA reconstituted in *E. coli* total membrane polar lipids (39), and with liquid-state NMR studies of *B. subtilis* $TatA_d$ and *E. coli* TatA reconstituted in DPC and $C_{12}E_9$ micelles (33,34).

Using SROCD and solid-state ^{15}N-NMR spectroscopy, we demonstrated here that the membrane alignment of $TatA_d$ is dramatically affected by hydrophobic mismatch and spontaneous bilayer curvature. The TMH can change its tilt angle and flip onto the membrane surface (where it remains well ordered or assembles into aggregates/clusters) depending on the bilayer thickness, spontaneous curvature, and the TMH length (see Fig. 2–5). When the membrane thickness is comparable with the hydrophobic length of the helix, the TMH is aligned in an essentially upright transmembrane orientation, as expected. In thinner membranes, the TMH is able to compensate the positive hydrophobic mismatch by increasing the tilt angle to prevent exposure of the hydrophobic side chains to the aqueous environment, as expected. However, aggregation/clustering is observed in membranes that are too thick, because the short TMH can no longer span the lipid bilayer, as neither the polar N-terminus (which is most likely charged under our NMR and OCD conditions) nor the APH can be pulled any deeper into the hydrophobic environment without energetic penalty. Our complementary SROCD analysis showed that $TatA_{2\text{-}45}$ forms aggregates/cluster in straight-chain phosphocholine membranes under negative hydrophobic mismatch, while maintaining its helical conformation throughout. This observation brought up the idea that TatA would be expelled from the hydrophobic membrane core under such conditions, and as a result ends up in the surface region of the lipid bilayer, where it has a tendency to self-assemble with a lack of any orientation preference. To demonstrate that the polarity and charge of the N-terminus play a critical role in the observed expulsion/aggregation of $TatA_{2\text{-}45}$ under negative hydrophobic mismatch, we prepared $TatA_{2\text{-}45}$ variants with additional charges in the N-terminal region. We found that these proteins started to aggregate already in relatively thin membranes as the additional charges are even less compatible with a hydrophobic environment. Thus, we suggest that the protonation state of the N-terminus in TatA can control the balance between its transmembrane alignment and a

surface-bound form (which tends to aggregate). This balance would be critical under conditions where the hydrophobic bilayer core is just about thick enough to accommodate the N-terminus in the deprotonated state but not in the protonated state. To observe this balance and avoid any aggregation near the membrane surface, we used branched-chain phytanoyl lipids with a highly negative spontaneous curvature. Our experimental data clearly show that the TMH of TatA gets flipped parallel to the membrane surface in a stable manner, such that the entire protein is accommodated near the loosely packed headgroup region of the phytanoyl lipids. MC simulations demonstrate that—in a membrane model of appropriate thickness—simple protonation of the TatA N-terminus is sufficient to flip the formerly inserted TMH out of its transmembrane state and into a surface-alignment just below the headgroup region.

The flipping of the TMH, yielding a horizontal surface-aligned orientation of the entire TatA protein would be expected to change the angle between the TMH and APH. If there exists a flexible hinge, then the TMH could swing straight out of the membrane core (see Fig. 8 *A*). In the case of rigid connection between the TMH and the APH, on the other hand, this would require a rotation of the entire protein (see Fig. 8 *B*). To date, it is not unambiguously known from the literature whether the "hinge region" is flexible or not. We had previously suggested that, for $TatA_{2\text{-}45}$, the short TMH pulls the connected end of the APH quite deeply into DMPC/DMPG bicelles, due to negative hydrophobic mismatch (32). The APH was found to be considerably tilted and at the same time its amphiphilic face was rotated at an unexpected and seemingly unfavorable azimuthal angle, which might imply that the hinge is rather rigid. However, we also have to consider that the connection between TMH and APH is very short (see Table 1); therefore, even a flexible hinge would lead to a similar scenario:

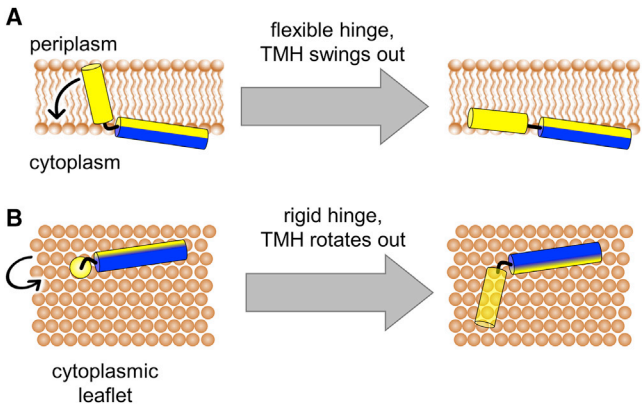

FIGURE 8 Possible flipping mechanism of the TatA TMH. Cartoon representation of $TatA_{2\text{-}45}$ with its membrane-spanning TMH (*yellow*) and its surface-bound APH (*blue-yellow*). (*A*) In the case of a flexible hinge, the TatA TMH could swing out of the membrane core. (*B*) In the case of a rigid linker region, the TatA TMH has to rotate out of the membrane core (view from the cytoplasmic leaflet). To see this figure in color, go online.

a pulling of the APH into the membrane. Our present MC simulations of $TatA_{1\text{-}45}$ indicate that the TMH can indeed swing out of the membrane core such that the entire molecule can stretch out more or less straight (see Fig. 6). Taken together, from these results and the unexpected azimuthal rotation angle of the APH from our previous study, it seems that the hinge can bend and straighten, although is probably limited in its flexibility to twist. We may at least conclude that it does not impose a rigid L-shape structure on the folded TatA protein.

Still, we have to consider how a TMH, when flipped parallel to the membrane surface, deals with the energetically unfavorable situation that hydrophobic side chains are exposed toward a more hydrophilic surrounding. In the MC simulations above, the flipped TMH is seen to adopt a banana-shaped structure. This is indeed plausible, as the polar N-terminal region (including the charged N-terminus) and the hinge region to the amphiphilic helix are drawn toward the hydrophilic environment, while the 12 hydrophobic residues of the TMH prefer the hydrophobic interior of the membrane. Remarkably, a very recent preprint (95) highlights the role of an N-terminal 4-residue motif directly in front of the 12 hydrophobic amino acids in all TatA proteins, which had not been noticed before, because the exact sequence differs between different species. This N-terminal motif possesses a "local amphipathic topology" and might introduce a "temporary hinge" at the extreme end of the N-terminus. So far, the role of this N-terminal motif is not clear, but, based on our results, it would help the flipped TatA TMH to be accommodated near the membrane surface. This may stabilize the partial immersion of those 12 hydrophobic residues near the hydrophobic membrane interior, while the more polar residues at the extreme N-terminal part point favorably into the hydrophilic environment. Furthermore, the conformation derived from our MD simulation suggests that additional stabilization is achieved by π-π stacking (86) and/or hydrophobic interactions between three Phe residues, which are positioned at the beginning, middle, and end of the TMH sequence of $TatA_d$ from *B. subtilis* (see Video S1). Only Phe21 at the end of the TMH is highly conserved in all TatA proteins (see Fig. S1); however, nonetheless, they all seem to possess at least one further aromatic residue in the N-terminal part of the TMH, which would probably also allow this kind of interaction. Notably, as Phe and other aromatic residues are most abundant at the edges of transmembrane segments as "anchoring" residues, they may conceivably also help to stabilize the TMH of TatA in the amphiphilic interphase when it has flipped to its surface-aligned state.

Our comprehensive structural analysis clearly shows that the TMH of TatA can flip out of the membrane core when it is triggered by negative hydrophobic mismatch, negative spontaneous bilayer curvature, or N-terminal TatA protonation. Such flipping of a hydrophobic transmembrane helix is obviously a rather unusual and unexpected behavior. Only

very few studies have reported so far that transmembrane helices can flip onto the membrane surface, based on hydrophobic mismatch, moderate hydrophobicity, pH shifts, or lipid headgroup charge (93,94,96–101). For example, a surface-aligned orientation of a 19-residue artificial TMH has been observed as a result of hydrophobic mismatch by fluorescence studies (102). Another example is the so-called pHLIP peptide (pH low insertion peptide), which folds and inserts into the membrane triggered by the pH value (103–108), although in this case a His-rich amphiphilic helix is being converted into a hydrophobic segment. Yet, it is conceivable that the flipping of genuinely hydrophobic helices has been underestimated so far, simply because this behavior is unexpected by the linguistic implication of a "TRANSmembrane" segment. In fact, helix flipping has been hypothesized to play an important role in the functional mechanism of several known membrane proteins. For example, in the lytic cycle of bacteriophages, pinholin $S^{21}68$ is supposed to be activated by a spontaneous flip response of its first TMH into the periplasm, allowing the assembly of small pinholes in the inner bacterial membrane. The resulting membrane depolarization then causes the TMH of yet another protein, the SAR-endolysin, to flip out of the membrane, which releases and activates the endolysin to degrade the cell wall (109–115). Furthermore, a flipping has been postulated for the protein 3A of the polio virus, which plays a role in its replication cycle (116). Lactose permease LacY, too, showed a flipped transmembrane segment upon changing its lipid environment (117). As discussed before, such flipping of a helical segment can be based on several structural properties of the helix, like moderate hydrophobicity or conformational flexibility. In the case of TatA, the short length of the TMH seems to be the crucial factor for its ability to flip, which can be also seen from the fact that variants with an extended TMH no longer flipped in phytanoyl lipids (see Fig. 5). In addition, the immediate proximity of the N-terminal amphiphilic motif and the near-neutral pKa of the N-terminus itself will assist to stabilize TatA in a flipped state when protonated.

To find out whether the short length of the TatA TMH is indeed necessary for successful translocation, we also performed an in vitro translocation assay on TatA variants with an elongated TMH (see Fig. 7). This way it was possible to prove that the unusually short length of the TMH is crucial for successful translocation of the natural *E. coli* Tat substrate AmiC into INVs. This finding is in perfect accordance with the fact that *Providencia stuartii* possesses a TatA protein with an extended TMH and can become activated only by cleavage of this N-terminal extension (118–120). Remarkably, two recent publications also investigated the role of the unusual short TMH for successful translocation, and their results are in perfect accordance with our study (53,54). These studies proved that the unusually short TatA TMH length is optimized for successful translocation, because increasing as well as reducing the TMH length leads to reduced transport activities in in vitro and in vivo assays. The TatA TMH length thus seems to be optimized for stable membrane insertion (presumably in its deprotonated state) and prevention of uncontrolled membrane destabilization/leakage on the one hand, while on the other hand it experiences sufficient negative hydrophobic mismatch in bacterial membranes to engage in the translocation process actively by flipping to the bilayer surface.

As an alternative interpretation, the reduced translocation activity which we and others have observed with increasing TMH length might be attributed to an inadequate alignment of the altered TatA TMH due to hydrophobic mismatch, which might hinder its interaction with TatC in the translocation cycle. However, our structural data show that the tilt angle of the extended TMH of TatA LAL is essentially the same as for the wild-type (see Fig. 3), whereas the translocation activity of this variant (and also the TatA LALA variant) is dramatically reduced (see Fig. 7). Furthermore, it has been recently shown that TatA variants with an increased TMH length possess a dominant negative effect when overexpressed in the presence of wild-type TatA, which proves that it can displace TatA wild-type from the TatA binding site on TatC (54). Therefore, we attribute the reduced translocation activity to the observed tighter hydrophobic anchoring of the variants with an elongated TMH (see Fig. 5).

What functional significance such a flipping TMH might have in the translocation process and how such a rearrangement of the TMH might be triggered in vivo is an intriguing question. TatA has been suggested to be involved in targeting of the cargo protein to the membrane and/or to the translocase, given that TatA has been found to exist also in a cytoplasmic soluble state (28,121–128). Therefore, a reversible integration of the short TMH into the membrane would seem feasible in the light of our findings. Compared with the surface-bound flipped state described here in our NMR and CD samples (which do not possess any excess hydration), an entirely free form of TatA without any membrane contact would certainly require an assembly of several molecules to compensate for the large hydrophobic surface that would otherwise be exposed to water. In that case it may well be feasible that the TMH interacts first with other TMH segments before binding the cargo protein, then the complex docks onto the membrane in a surface-bound state, before finally being inserted all the way across the membrane upon deprotonation of the N-terminus. As we have shown that an elongation of the TMH by only three residues abolishes the expulsion from a membrane nearly completely, it seems that the TatA TMH has the perfect length for a—possibly reversible—integration into the native bacterial membrane. TatA proteins from other species have similarly short helices, so this characteristic feature is evolutionarily conserved (see Fig. S1 and (53,54)).

Besides a possible role in the recruitment of cargo to the membrane, it is interesting to speculate whether the TMH might be involved in any important step during the translocation process. The considerable structural rearrangement induced by the flip could, for example, trigger the formation of a pore or a membrane defect. The short TMH of TatA has been suggested to play an active role in the translocation process (34,48,53,54), because it induces negative hydrophobic mismatch that would destabilize the membrane. Based on this membrane-weakening model, the N-terminal part of the APH gets pulled quite deeply inside the membrane to compensate for the negative hydrophobic mismatch in the inactive state, as suggested from our previous solid-state NMR analysis (32). An interaction with TatBC or binding of the cargo protein leads then to a rearrangement of the APH toward the membrane surface, which pulls the polar N-terminus of the TMH inside the membrane, leading to membrane thinning and destabilization due to the pronounced negative hydrophobic mismatch. Interestingly, the groups of Brüser and Theg (48,53,54) could furthermore show that the short TatA TMH alone can destabilize membranes and induce proton leakage in vitro, and strikingly this behavior was based only on its shortness, irrespective of the actual TMH sequence. Our work supports the concepts of the recent studies, and our results are in full agreement with the findings (48,53,54). In addition, our concept of a flipping TMH and its first experimental demonstration under negative hydrophobic mismatch conditions can explain the observed destabilization of the membrane.

Furthermore, we have shown here that the charge of the N-terminus plays a critical role in the observed flipping of the TMH. It is well known that Tat-dependent transport is driven by the proton-motive force across the membrane. Therefore, we suggest that protonation of the N-terminus could actually drive the flipping and thereby equilibrate the proton gradient across the membrane in an active manner. This concept would explain the proton leakage observed by Hou et al. upon adding merely the TMH to membranes (48). A pH-driven rearrangement of the TMH during the translocation process would also provide an explanation for the puzzling topology of the TatA N-terminus, which has been suggested in early reports to face the inside of the cell (44), whereas it is now generally agreed that it faces toward the outside (129). According to our model, both observations should be possible, depending on the state of the translocation cycle.

CONCLUSIONS

Combining all these results, we speculate that Tat-dependent translocation in *B. subtilis* involves the following stages illustrated in Fig. 9 (after the cargo has been recruited, which also needs to be attached to TatC). In an inactive starting state, the TatA TMH is stably inserted upright across the membrane (i.e., as a genuine transmembrane helix), keeping

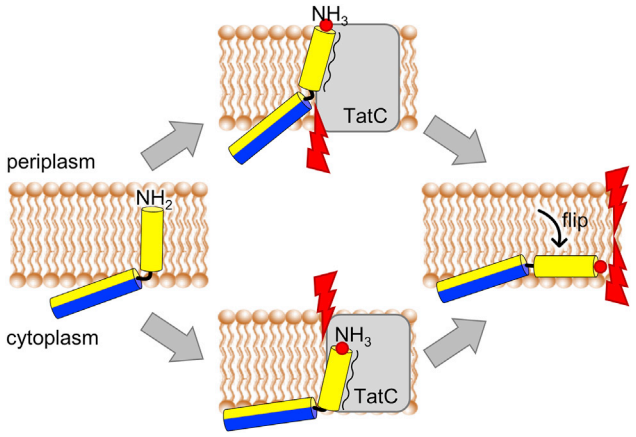

FIGURE 9 Speculative model of TatA TMH flipping triggered by TatC. Cartoon representation of $TatA_{2\text{-}45}$ with its hydrophobic TMH (*yellow*) and its amphiphilic APH (*blue-yellow*). At the start, the TMH of TatA is inserted in an upright transmembrane state, with both the unprotonated N-terminus and the APH immersed sufficiently deep into the membrane core to just about tolerate the hydrophobic mismatch (*left panel*). Interaction of TatA with its binding site on TatC (indicated by the *squiggly line*) leads to protonation of the N-terminus (indicated by *red dots*). The increased polarity leads to stronger hydrophobic mismatch (indicated by *red flashes*) either at the extracellular face (*upper panel*) or on the cytoplastic face (*lower panel*) or both. This strain results in flipping of the protonated TMH toward the cytoplasmic membrane surface (*right panel*), leading to local membrane weakening and/or permeation, especially if several TatA molecules participate. To see this figure in color, go online.

both the deprotonated N-terminus and the APH quite deeply immersed, just about tolerating the hydrophobic mismatch (32,34,48,53). Due to the known interaction of TatA with the surface of TatC, the TMH and/or the APH could be pulled more deeply inside the membrane (34,48,53). The resulting hydrophobic mismatch would be even more pronounced if the TMH gets protonated at the extracellular membrane surface in the course of its interaction with TatC. The postulated binding site of TatA to TatC has been sketched in Fig. 9 according to the crystal structure of TaC, where the docking of TatA (and the homologous TatB protein) to TatC has been described (31,35,36). The exact depth at which TatA binds to TatC, relative to the lipid membrane, however, would still need to be modeled more carefully with regard to our present model. Nonetheless, either scenario (*upper* or *lower* panel in Fig. 9, or anything in between) leads to enhanced hydrophobic mismatch, which should result in a flipping of the TMH toward the cytoplasmic face of the membrane. If the N-terminus is protonated in this step, the direction of this inward flip will be naturally promoted by the proton motive force. Altogether, such sequence of events may cause enough membrane destabilization to initiate translocation at the TatC interface (5,31,48,53). It may well be a cumulative process involving several TMH segments, since TatA is known to be present in the membrane in a preassembled oligomeric state (14,24,26–28,53). The detailed structure and functional mechanism of such a membrane-weakening TatA cluster

still need to be determined. It is conceivable that a toroidal pore is formed due to the TatA-induced membrane thinning/damage, as proposed by the group of Theg et al. (54), or a that a row of TatA molecules permit the passage of the cargo protein as proposed by Brüser and co-workers (53). In any of these scenarios, a flipping of the protonated TMH could be the final step of membrane destabilization.

MATERIALS AND METHODS

TatA constructs

All structural investigations were carried out with a C-terminally truncated $TatA_{2\text{-}45}$ construct and several variants thereof (for sequences, see Table 1). The mutations were introduced into the plasmid pET28 $TatA_{1\text{-}45}$ (40), which contains the wild-type $TatA_{1\text{-}45}$ sequence with an N-terminal His_6-tag to facilitate purification (yielding the construct $TatA_{2\text{-}45}$ after BrCN cleavage of the His_6-tag). For the in vitro translocation assay, the *E. coli* TatA variants with an extended TMH were produced based on the plasmid pET22b + TatABCD (= p8737), which allows the overexpression of TatA, TatB, TatC, and TatD in *E. coli* BL21 (DE3) strains (130). All mutagenesis was performed using the QuikChange Site-Directed Mutagenesis Kit (Stratagene/Agilent Technologies, Waldbronn, Germany) according to the protocol of the manufacturer. Oligonucleotide primers were purchased from Eurofins (Ebersberg, Germany), and the DNA sequence of each mutant was verified by sequencing (GATC Biotech, Konstanz, Germany). The template plasmids and primers can be found in Table S1 of the supporting material.

Expression and purification of $TatA_{2\text{-}45}$ constructs

The $TatA_{2\text{-}45}$ constructs were expressed (both unlabeled for CD spectroscopy and uniform ^{15}N-labeled for NMR spectroscopy) and purified as described previously (32,40,41). The identity and purity of the constructs were checked by MALDI-TOF mass spectrometry (Autoflex III, Bruker, Billerica, MA) and SDS-PAGE (Mini-PROTEAN Tetra Cell, Bio-Rad Laboratories, Munich, Germany).

Lipids

For reconstitution of the protein the phosphatidylcholine lipids shown in Table 2 were used, namely the saturated lipids DOcPC, DDPC, DLPC, and DMPC, and the unsaturated lipids DOPC, DEiPC, DErPC, and DNPC. In addition, the branched phytanoyl lipids DPhPC and DPhPE were used. All lipids were purchased from Avanti Polar Lipids (Alabaster, AL).

SRCD and SROCD spectroscopy

SRCD and SROCD sample preparation was performed as basically described previously (40). For SRCD samples, $TatA_{2\text{-}45}$ and its variants were reconstituted in small unilamellar vesicles (SUVs) made of the lipids shown in Table 2 with a protein-to-lipid (P/L) ratio of 1:50 (mol/mol). Purified protein and lipid powder were codissolved in HFIP and sonicated for at least 5 min to get a clear solution. Subsequently, the organic solvent was removed by a gentle stream of nitrogen and the sample was stored under reduced pressure overnight. The dry protein-lipid film was rehydrated by addition of 25 μL water and sonication. Then, several freeze-thaw cycles (40°C for 10 min and −196°C for 10 min) were performed, followed by sonication at maximal power to generate SUVs. The SUVs were kept above their lipid phase transition temperature the whole time. Finally, a 4 μL aliquot of the sample (containing 16 μg protein) was filled into a "Birkbeck-type" demountable calcium fluoride cell (131) with an optical pathlength of 12.2 μm.

For SROCD samples, the $TatA_{2\text{-}45}$ constructs were reconstituted in macroscopically aligned lipid bilayers made of the lipids shown in Table 2 with a P/L ratio of 1:50 (mol/mol). Purified protein and lipid powder were codissolved in HFIP. Subsequently, an aliquot (containing 50–150 μg lipid) was deposited onto a 20 mm diameter quartz glass plate with a 12 mm spot diameter, and allowed to dry in a gentle stream of air until the sample appeared dry. The plate was kept under vacuum for 2 h to remove residual organic solvent. Then the sample was hydrated overnight at 30°C and 97% relative humidity using saturated potassium sulfate (K_2SO_4) solution. During hydration the lipids spontaneously align as multilamellar bilayers parallel to the quartz glass plate surface. Finally, the oriented sample was assembled perpendicular to the incident light beam in the SROCD measurement cell.

SRCD and SROCD measurements were performed on the UV-CD12 beamline at ANKA. The beamline components and its experimental equipment have been described in detail by Clarke and Jones (132) as well as Bürck et al. (61). SRCD spectra were recorded at 35°C and SROCD spectra at 30°C. The temperature of the SRCD measurements was controlled by Peltier elements, whereas the SROCD measurements were controlled by a water thermostat. SRCD spectra were recorded between 260 and 180 nm with a scan rate of 20 nm per min at 0.5 nm intervals. Three repeat scans were averaged for each sample, using a 1 nm bandwidth, a 300 ms lock-in time, and a 1500 ms dwell time. SROCD spectra were recorded every 45° of cell rotation from 260 to 180 nm to reduce possible spectral artifacts caused by the linear dichroism arising from imperfections in the sample, strain in the quartz glass windows, or imperfect alignment of the windows. The resulting eight spectra were measured at 0.5 nm wavelength steps and 1500 ms dwell time. All eight spectra were subsequently averaged. For baseline correction of the SROCD and SRCD measurements a protein-free lipid sample was measured under the same conditions and subtracted from the protein spectrum.

No mean residue ellipticity values were calculated, because the protein concentration of the samples could not be determined with the necessary accuracy by standard colorimetric assays. UV concentration determination at 280 nm could not be performed because $TatA_{2\text{-}45}$ possesses no UV-absorbing tryptophan or tyrosine residues. Postprocessing and smoothing of SRCD raw data was performed with the CDtool software package (133), and the final corrected spectra were compared with a basic set of CD spectra of pure secondary structural elements (134). The global minima of the SROCD spectra were scaled to the same intensity and the SRCD spectra in Figs. S3–S5 were normalized at 223 nm to allow direct comparison of the line shapes.

Solid-state NMR spectroscopy

For solid-state NMR samples, the $TatA_{2\text{-}45}$ variants were reconstituted in macroscopically aligned lipid bilayers with a P/L ratio of 1:75 (mol/mol). Purified protein and lipid powder were codissolved in HFIP and sonicated for at least 5 min to get a clear solution (containing 18.9 mg lipid). Subsequently, the solution was evenly spotted onto 20 glass plates ($7.5 \times 12 \times 0.06$ mm^3; Marienfeld, Germany) and allowed to dry in a gentle stream of air until the sample appeared dry. Then the glass plates were kept under vacuum overnight to remove residual organic solvent. Afterward, the glass plates were stacked and hydrated overnight at 48°C and 97% relative humidity using a saturated K_2SO_4 solution. Finally, the glass plate stack was wrapped into parafilm and polyethylene foil to avoid drying-out during the NMR measurement.

1D solid-state NMR experiments were performed on an Avance III spectrometer (Bruker) equipped with a wide-bore 500 MHz magnet. The spectra were acquired using a double-tuned $^1H/^{15}N$-probe with a low-E flat-coil resonator or a triple-tuned $^1H/X/Y$-probe (Bruker). The quality of the lipid

alignment was checked by ^{31}P-NMR experiments before and after each ^{15}N-NMR measurement. The membrane alignment of the proteins was determined by 1D ^{15}N-NMR experiments. The temperature was set to 35°C to stay above the lipid phase transition temperature of all used lipids, with the exception of the DPhPC/DPhPE containing samples that were measured at 22°C to avoid drying-out which would enhance the risk of a hexagonal lipid phase transition (85). All spectra were recorded with cross-polarization using a CPMOIST pulse sequence (135) to compensate radio frequency power mismatches or with the RAMP-CP pulse sequence (136) (80% ramp) to increase meeting the Hartmann-Hahn match conditions. Heteronuclear ^{1}H-decoupling was achieved during acquisition using an SPINAL-16 composite pulse sequence (137,138) with a field strength of 30 kHz. A cross-polarization contact time of 1 ms was used and a recycle delay of 6–8 s to avoid sample heating. The ^{1}H-carrier frequency was set to 9 ppm and the ^{15}N-carrier frequency to 110 ppm. ^{15}N-chemical shift frequencies were referenced to solid ammonium sulfate (26.8 ppm), and ^{1}H-chemical shift frequencies were referenced to H_2O (4.7 ppm at 42°C). Data were processed and displayed using the software TOPSPIN (Bruker).

MC simulations

In the all-atom MC simulations we parameterized the protein fragment $TatA_{1\text{-}45}$ in the AMBER99SB-ILDN* force field (139) using the SIMONA framework (140). The APH was placed on the membrane surface and the TMH inserted into the membrane with a deprotonated or protonated N-terminus, respectively. The implicit membrane model used here (141) combines advantages of two established implicit membrane models (142,143) that are based on the generalized Born formalism (144) with an efficient and accurate generalized Born implementation for aqueous solutions (145). The membrane is modeled using a dielectric slab (143) representing the hydrophobic core (42 Å thickness with relative dielectric constant $\varepsilon_{core} = 2$), the more polar headgroup regions (4 Å thickness with relative dielectric constant of $\varepsilon_{head} = 6$), and the surrounding water ($\varepsilon_{water} = 80$). We chose $\varepsilon_{protein} = 2$, the same value as for the membrane core region. The free energy change of transferring a charged atom from water into the membrane is approximated by computing the transfer between the different slabs separately, as given by

$$\Delta G(water \leftrightarrow membrane) \approx \Delta G(water \leftrightarrow headgroup) + \Delta G(headgroup \leftrightarrow core).$$

This model also accounts accurately for the orientation of nonpolar protein regions with respect to the membrane by using the method proposed in Spassov et al. (142), incorporating a dielectric slab into the Born radii of the generalized Born model. Additional nonpolar contributions are modeled by a solvent-accessible surface area term that is scaled depending on the position inside the membrane (143).

MC simulations were performed at 300 K in 20 independent simulations per system, totalling 200 million steps. The forces and energy calculations were implemented as described previously (141). In each MC step either one dihedral angle (backbone or side chain) or a sequence of adjacent backbone angles was changed, or a translation or rotation of an entire molecule was performed. These movements were drawn from Gaussian distributions with standard deviations of 20° for backbone and side-chain angles, 5° for rotation, and 1.4 Å for translation.

In vitro translocation assay

The in vitro translocation assay was performed as described by Moser et al. (87). In brief, inverted membrane vesicles were prepared from a TatABCD overproducing *E. coli* strain (*E. coli* BL21 [DE3] ΔTat [kindly provided by B. Ize and T. Palmer] complemented with the respective plasmid pET22b + TatABCD). The natural *E. coli* Tat substrate AmiC was synthesized and radioactively labeled via in vitro transcription/translation. The INVs were added 10 min after starting the synthesis reaction of AmiC, and incubated for 25 min at 37°C. For assaying the translocation of the substrate into the INVs, one part of each reaction was treated directly with 10% (w/v) trichloroacetic acid to precipitate the protein, and the other part was treated with PK at 25°C for 20 min before trichloroacetic acid precipitation. The precipitated protein was pelleted by centrifugation and analyzed using SDS-PAGE and phosphor imaging. The presence of TatA, TatB, and TatC in the prepared INVs was checked using a Western blot with the corresponding antibodies, as described in Blümmel et al. (146).

SUPPORTING MATERIAL

Supporting material can be found online at https://doi.org/10.1016/j.bpj.2022.12.016.

AUTHOR CONTRIBUTIONS

E.R.S., L.M.E.S., and T.H.W. wrote the manuscript and A.S.U. revised it. S.V. and C.G. did the mutagenesis of the $TatA_d$ constructs. E.R.S. and L.M.E.S. did the recombinant protein expression and performed SR(O)CD measurements. J.B. and T.H.W. supervised the CD measurements. E.R.S. performed the solid-state NMR measurements and S.L.G. and T.H.W. supervised the NMR part. S.A. performed MALDI-TOF mass spectrometry. J.S. performed the MC simulations and W.W. supervised the simulations. J.F. and A.-S.B. performed the in vitro translocation assays. A.S.U. conceived and T.H.W. coordinated the project.

ACKNOWLEDGMENTS

We acknowledge the KIT light source for providing instrumentation at the beamline UV-CD12 of the Institute of Biological Interfaces (IBG2), and we thank the Institute for Beam Physics and Technology (IBPT) for operating the storage ring KARA (Karlsruhe Research Accelerator), as well as Bianca Posselt and Siegmar Roth for their assistance with the SRCD/SROCD measurements. We acknowledge funding by the Helmholtz program "Natural, Artificial and Cognitive Information Processing (NACIP)." We are grateful to the DFG project "INST 121384/58-1 FUGG" for providing financial support for our NMR equipment, and we thank Markus Schmitt for technical assistance with the NMR equipment. T.H.W. acknowledges financial support by a YIG grant (KIT Karlsruhe, Germany) and C.G. acknowledges financial support by a grant of the MWK Baden-Württemberg. We also thank Matthias Müller (University of Freiburg) for fruitful discussions.

DECLARATION OF INTERESTS

The authors declare no competing interests.

SUPPORTING CITATIONS

References (147,148) appear in the supporting material.

REFERENCES

1. Goosens, V. J., and J. M. van Dijl. 2016. Twin-arginine protein translocation. *In* Curr Top Microbiol Immunol.. Springer Berlin Heidelberg, Berlin, Heidelberg, pp. 1–26.
2. Berks, B. C. 2015. The twin-arginine protein translocation pathway. *Annu. Rev. Biochem.* 84:843–864.
3. Patel, R., S. M. Smith, and C. Robinson. 2014. Protein transport by the bacterial Tat pathway. *Biochim. Biophys. Acta.* 1843:1620–1628.

4. Goosens, V. J., C. G. Monteferrante, and J. M. van Dijl. 2014. The Tat system of Gram-positive bacteria. *Biochim. Biophys. Acta.* 1843:1698–1706.
5. Fröbel, J., P. Rose, and M. Müller. 2012. Twin-arginine-dependent translocation of folded proteins. *Philos. Trans. R. Soc. Lond. B Biol. Sci.* 367:1029–1046.
6. Cline, K. 2015. Mechanistic aspects of folded protein transport by the twin arginine translocase (tat). *J. Biol. Chem.* 290:16530–16538.
7. Freudl, R. 2013. Leaving home ain't easy: protein export systems in Gram-positive bacteria. *Res. Microbiol.* 164:664–674.
8. Palmer, T., and B. C. Berks. 2012. The twin-arginine translocation (Tat) protein export pathway. *Nat. Rev. Microbiol.* 10:483–496.
9. Sargent, F., E. G. Bogsch, …, T. Palmer. 1998. Overlapping functions of components of a bacterial Sec-independent protein export pathway. *EMBO J.* 17:3640–3650.
10. Dilks, K., R. W. Rose, …, M. Pohlschröder. 2003. Prokaryotic utilization of the twin-arginine translocation pathway: a genomic survey. *J. Bacteriol.* 185:1478–1483.
11. Yen, M.-R., Y. H. Tseng, …, M. H. Saier, Jr. 2002. Sequence and phylogenetic analyses of the twin-arginine targeting (Tat) protein export system. *Arch. Microbiol.* 177:441–450.
12. Jongbloed, J. D. H., U. Grieger, …, J. M. van Dijl. 2004. Two minimal Tat translocases in Bacillus. *Mol. Microbiol.* 54:1319–1325.
13. Pop, O., U. Martin, …, J. P. Müller. 2002. The twin-arginine signal peptide of PhoD and the TatAd/Cd proteins of Bacillus subtilis form an autonomous Tat translocation system. *J. Biol. Chem.* 277:3268–3273.
14. Barnett, J. P., R. T. Eijlander, …, C. Robinson. 2008. A minimal tat system from a Gram-positive organism. *J. Biol. Chem.* 283:2534–2542.
15. Blaudeck, N., P. Kreutzenbeck, …, R. Freudl. 2005. Isolation and characterization of bifunctional Escherichia coli TatA mutant proteins that allow efficient Tat-dependent protein translocation in the absence of TatB. *J. Biol. Chem.* 280:3426–3432.
16. Holzapfel, E., G. Eisner, …, M. Müller. 2007. The entire N-terminal half of TatC is involved in twin-arginine precursor binding. *Biochemistry.* 46:2892–2898.
17. Cline, K., and H. Mori. 2001. Thylakoid DeltapH-dependent precursor proteins bind to a cpTatC-Hcf106 complex before Tha4-dependent transport. *J. Cell Biol.* 154:719–729.
18. Lausberg, F., S. Fleckenstein, …, R. Freudl. 2012. Genetic evidence for a tight cooperation of TatB and TatC during productive recognition of twin-arginine (Tat) signal peptides in Escherichia coli. *PLoS One.* 7:e39867.
19. Kreutzenbeck, P., C. Kröger, …, R. Freudl. 2007. Escherichia coli twin arginine (Tat) mutant translocases possessing relaxed signal peptide recognition specificities. *J. Biol. Chem.* 282:7903–7911.
20. Strauch, E. M., and G. Georgiou. 2007. Escherichia coli tatC mutations that suppress defective twin-arginine transporter signal peptides. *J. Mol. Biol.* 374:283–291.
21. Orriss, G. L., M. J. Tarry, …, B. C. Berks. 2007. TatBC, TatB, and TatC form structurally autonomous units within the twin arginine protein transport system of Escherichia coli. *FEBS Lett.* 581:4091–4097.
22. Alami, M., I. Lüke, …, M. Müller. 2003. Differential interactions between a twin-arginine signal peptide and its translocase in Escherichia coli. *Mol. Cell.* 12:937–946.
23. Tarry, M. J., E. Schäfer, …, B. C. Berks. 2009. Structural analysis of substrate binding by the TatBC component of the twin-arginine protein transport system. *Proc. Natl. Acad. Sci. USA.* 106:13284–13289.
24. Gohlke, U., L. Pullan, …, B. C. Berks. 2005. The TatA component of the twin-arginine protein transport system forms channel complexes of variable diameter. *Proc. Natl. Acad. Sci. USA.* 102:10482–10486.
25. Jack, R. L., F. Sargent, …, T. Palmer. 2001. Constitutive expression of Escherichia coli tat genes indicates an important role for the Twin-Arginine Translocase during aerobic and anaerobic growth. *J. Bacteriol.* 183:1801–1804.
26. Sargent, F., U. Gohlke, …, B. C. Berks. 2001. Purified components of the Escherichia coli Tat protein transport system form a double-layered ring structure. *Eur. J. Biochem.* 268:3361–3367.
27. Oates, J., C. M. L. Barrett, …, C. Robinson. 2005. The Escherichia coli twin-arginine translocation apparatus incorporates a distinct form of TatABC complex, spectrum of modular TatA complexes and minor TatAB complex. *J. Mol. Biol.* 346:295–305.
28. Westermann, M., O. I. Pop, …, J. P. Müller. 2006. The TatAd component of the Bacillus subtilis twin-arginine protein transport system forms homo-multimeric complexes in its cytosolic and membrane embedded localisation. *Biochim. Biophys. Acta.* 1758:443–451.
29. Walther, T. H., C. Gottselig, …, A. S. Ulrich. 2013. Folding and self-assembly of the TatA translocation pore based on a charge zipper mechanism. *Cell.* 152:316–326.
30. Fröbel, J., P. Rose, …, M. Müller. 2012. Transmembrane insertion of twin-arginine signal peptides is driven by TatC and regulated by TatB. *Nat. Commun.* 3:1311.
31. Alcock, F., P. J. Stansfeld, …, B. C. Berks. 2016. Assembling the Tat protein translocase. *Elife.* 5:e20718.
32. Walther, T. H., S. L. Grage, …, A. S. Ulrich. 2010. Membrane alignment of the pore-forming component $TatA_d$ of the twin-arginine translocase from Bacillus subtilis resolved by solid-state NMR spectroscopy. *J. Am. Chem. Soc.* 132:15945–15956.
33. Hu, Y., E. Zhao, …, C. Jin. 2010. Solution NMR structure of the TatA component of the twin-arginine protein transport system from Gram-positive bacterium Bacillus subtilis. *J. Am. Chem. Soc.* 132:15942–15944.
34. Rodriguez, F., S. L. Rouse, …, J. R. Schnell. 2013. Structural model for the protein-translocating element of the twin-arginine transport system. *Proc. Natl. Acad. Sci. USA.* 110:E1092–E1101.
35. Rollauer, S. E., M. J. Tarry, …, S. M. Lea. 2012. Structure of the TatC core of the twin-arginine protein transport system. *Nature.* 492:210–214.
36. Ramasamy, S., R. Abrol, …, W. M. Clemons, Jr. 2013. The glove-like structure of the conserved membrane protein TatC provides insight into signal sequence recognition in twin-arginine translocation. *Structure.* 21:777–788.
37. Zhang, Y., L. Wang, …, C. Jin. 2014. Solution structure of the TatB component of the twin-arginine translocation system. *Biochim. Biophys. Acta.* 1838:1881–1888.
38. Zhang, Y., Y. Hu, …, C. Jin. 2014. Structural basis for TatA oligomerization: an NMR study of Escherichia coli TatA dimeric structure. *PLoS One.* 9:e103157.
39. Porcelli, I., E. de Leeuw, …, B. C. Berks. 2002. Characterization and membrane assembly of the TatA component of the Escherichia coli twin-arginine protein transport system. *Biochemistry.* 41:13690–13697.
40. Lange, C., S. D. Müller, …, A. S. Ulrich. 2007. Structure analysis of the protein translocating channel TatA in membranes using a multi-construct approach. *Biochim. Biophys. Acta.* 1768:2627–2634.
41. Müller, S. D., A. A. De Angelis, …, A. S. Ulrich. 2007. Structural characterization of the pore forming protein TatAd of the twin-arginine translocase in membranes by solid-state ^{15}N-NMR. *Biochim. Biophys. Acta.* 1768:3071–3079.
42. Lee, P. A., G. Buchanan, …, T. Palmer. 2002. Truncation analysis of TatA and TatB defines the minimal functional units required for protein translocation. *J. Bacteriol.* 184:5871–5879.
43. Dabney-Smith, C., H. Mori, and K. Cline. 2006. Oligomers of Tha4 organize at the thylakoid Tat translocase during protein transport. *J. Biol. Chem.* 281:5476–5483.
44. Chan, C. S., M. R. Zlomislic, …, R. J. Turner. 2007. The TatA subunit of Escherichia coli twin-arginine translocase has an N-in topology. *Biochemistry.* 46:7396–7404.
45. Gouffi, K., F. Gérard, …, L. F. Wu. 2004. Dual topology of the Escherichia coli TatA protein. *J. Biol. Chem.* 279:11608–11615.

46. Berks, B. C., F. Sargent, and T. Palmer. 2000. The Tat protein export pathway. *Mol. Microbiol.* 35:260–274.

47. Brüser, T., and C. Sanders. 2003. An alternative model of the twin arginine translocation system. *Microbiol. Res.* 158:7–17.

48. Hou, B., E. S. Heidrich, …, T. Brüser. 2018. The TatA component of the twin-arginine translocation system locally weakens the cytoplasmic membrane of Escherichia coli upon protein substrate binding. *J. Biol. Chem.* 293:7592–7605.

49. Rohl, C. A., A. Chakrabartty, and R. L. Baldwin. 1996. Helix propagation and N-cap propensities of the amino acids measured in alanine-based peptides in 40 volume percent trifluoroethanol. *Protein Sci.* 5:2623–2637.

50. de Planque, M. R. R., B. B. Bonev, …, J. A. Killian. 2003. Interfacial anchor properties of tryptophan residues in transmembrane peptides can dominate over hydrophobic matching effects in Peptide−Lipid interactions. *Biochemistry.* 42:5341–5348.

51. de Jesus, A. J., and T. W. Allen. 2013. The role of tryptophan side chains in membrane protein anchoring and hydrophobic mismatch. *Biochim. Biophys. Acta.* 1828:864–876.

52. Windisch, D., C. Ziegler, …, A. S. Ulrich. 2015. Hydrophobic mismatch drives the interaction of E5 with the transmembrane segment of PDGF receptor. *Biophys. J.* 109:737–749.

53. Mehner-Breitfeld, D., M. T. Ringel, …, T. Brüser. 2022. TatA and TatB generate a hydrophobic mismatch important for the function and assembly of the Tat translocon in Escherichia coli. *J. Biol. Chem.* 298:102236.

54. Hao, B., W. Zhou, and S. M. Theg. 2022. Hydrophobic mismatch is a key factor in protein transport across lipid bilayer membranes via the Tat pathway. *J. Biol. Chem.* 298:101991.

55. Beck, D., N. Vasisht, …, C. J. Smith. 2013. Ultrastructural characterisation of Bacillus subtilis TatA complexes suggests they are too small to form homooligomeric translocation pores. *Biochim. Biophys. Acta.* 1833:1811–1819.

56. Marsh, D. 2008. Energetics of hydrophobic matching in lipid-protein interactions. *Biophys. J.* 94:3996–4013.

57. Tristram-Nagle, S., D. J. Kim, …, J. F. Nagle. 2010. Structure and water permeability of fully hydrated diphytanoylPC. *Chem. Phys. Lipids.* 163:630–637.

58. Grau-Campistany, A., E. Strandberg, …, A. S. Ulrich. 2015. Hydrophobic mismatch demonstrated for membranolytic peptides and their use as molecular rulers to measure bilayer thickness in native cells. *Sci. Rep.* 5:9388.

59. Pluhackova, K., and A. Horner. 2021. Native-like membrane models of E. coli polar lipid extract shed light on the importance of lipid composition complexity. *BMC Biol.* 19:4.

60. Miles, A. J., and B. A. Wallace. 2006. Synchrotron radiation circular dichroism spectroscopy of proteins and applications in structural and functional genomics. *Chem. Soc. Rev.* 35:39–51.

61. Bürck, J., S. Roth, …, A. S. Ulrich. 2015. UV-CD12: synchrotron radiation circular dichroism beamline at ANKA. *J. Synchrotron Radiat.* 22 (Pt 3):844–852.

62. Wallace, B. A., and D. Mao. 1984. Circular dichroism analyses of membrane proteins: an examination of differential light scattering and absorption flattening effects in large membrane vesicles and membrane sheets. *Anal. Biochem.* 142:317–328.

63. Bürck, J., P. Wadhwani, …, A. S. Ulrich. 2016. Oriented circular dichroism: a method to characterize membrane-active peptides in oriented lipid bilayers. *Acc. Chem. Res.* 49:184–192.

64. Bürck, J., S. Roth, …, A. S. Ulrich. 2008. Conformation and membrane orientation of amphiphilic helical peptides by oriented circular dichroism. *Biophys. J.* 95:3872–3881.

65. Muhle-Goll, C., S. Hoffmann, …, A. S. Ulrich. 2012. Hydrophobic matching controls the tilt and stability of the dimeric platelet-derived growth factor receptor (PDGFR) β transmembrane segment. *J. Biol. Chem.* 287:26178–26186.

66. Nolandt, O. V., T. H. Walther, …, A. S. Ulrich. 2009. Structure analysis of the membrane protein TatC(d) from the Tat system of B. subtilis by circular dichroism. *Biochim. Biophys. Acta.* 1788:2238–2244.

67. Klein, M. J., S. L. Grage, …, A. S. Ulrich. 2012. Structure analysis of the membrane-bound PhoD signal peptide of the Tat translocase shows an N-terminal amphiphilic helix. *Biochim. Biophys. Acta.* 1818:3025–3031.

68. Windisch, D., C. Ziegler, …, A. S. Ulrich. 2014. Structural characterization of a C-terminally truncated E5 oncoprotein from papillomavirus in lipid bilayers. *Biol. Chem.* 395:1443–1452.

69. Marassi, F. M., A. Ramamoorthy, and S. J. Opella. 1997. Complete resolution of the solid-state NMR spectrum of a uniformly 15N-labeled membrane protein in phospholipid bilayers. *Proc. Natl. Acad. Sci. USA.* 94:8551–8556.

70. Ridone, P., S. L. Grage, B. Martinac…, 2018. "Force-from-lipids" gating of mechanosensitive channels modulated by PUFAs. *J. Mech. Behav. Biomed. Mater.* 79:158–167.

71. Grage, S. L., A. M. Keleshian, …, B. Martinac. 2011. Bilayer-mediated clustering and functional interaction of MscL channels. *Biophys. J.* 100:1252–1260.

72. Strandberg, E., S. Esteban-Martín, …, J. Salgado. 2012. Hydrophobic mismatch of mobile transmembrane helices: merging theory and experiments. *Biochim. Biophys. Acta.* 1818:1242–1249.

73. Killian, J. A. 1998. Hydrophobic mismatch between proteins and lipids in membranes. *Biochim. Biophys. Acta.* 1376:401–415.

74. Wu, Y., H. W. Huang, and G. A. Olah. 1990. Method of oriented circular dichroism. *Biophys. J.* 57:797–806.

75. Grimsley, G. R., J. M. Scholtz, and C. N. Pace. 2009. A summary of the measured pK values of the ionizable groups in folded proteins. *Protein Sci.* 18:247–251.

76. Strandberg, E., D. Tiltak, …, A. S. Ulrich. 2012. Lipid shape is a key factor for membrane interactions of amphipathic helical peptides. *Biochim. Biophys. Acta.* 1818:1764–1776.

77. Zamora-Carreras, H., E. Strandberg, …, A. S. Ulrich. 2016. Alanine scan and ^{2}H NMR analysis of the membrane-active peptide BP100 point to a distinct carpet mechanism of action. *Biochim. Biophys. Acta.* 1858:1328–1338.

78. Grau-Campistany, A., E. Strandberg, …, A. S. Ulrich. 2016. Extending the hydrophobic mismatch concept to amphiphilic membranolytic peptides. *J. Phys. Chem. Lett.* 7:1116–1120.

79. Afonin, S., R. W. Glaser, …, A. S. Ulrich. 2014. ^{19}F NMR screening of unrelated antimicrobial peptides shows that membrane interactions are largely governed by lipids. *Biochim. Biophys. Acta.* 1838: 2260–2268.

80. Strandberg, E., J. Zerweck, …, A. S. Ulrich. 2013. Synergistic insertion of antimicrobial magainin-family peptides in membranes depends on the lipid spontaneous curvature. *Biophys. J.* 104:L9–L11.

81. Strandberg, E., A. Grau-Campistany, …, A. S. Ulrich. 2018. Helix fraying and lipid-dependent structure of a short amphipathic membrane-bound peptide revealed by solid-state NMR. *J. Phys. Chem. B.* 122:6236–6250.

82. Gagnon, M.-C., E. Strandberg, …, A. S. Ulrich. 2017. Influence of the length and charge on the activity of α-helical amphipathic antimicrobial peptides. *Biochemistry.* 56:1680–1695.

83. Strandberg, E., and A. S. Ulrich. 2015. AMPs and OMPs: is the folding and bilayer insertion of β-stranded outer membrane proteins governed by the same biophysical principles as for α-helical antimicrobial peptides? *Biochim. Biophys. Acta.* 1848:1944–1954.

84. Kara, S., S. Afonin, …, A. S. Ulrich. 2017. Diphytanoyl lipids as model systems for studying membrane-active peptides. *Biochim. Biophys. Acta Biomembr.* 1859:1828–1837.

85. Hsieh, C. H., S. C. Sue, …, W. G. Wu. 1997. Membrane packing geometry of diphytanoylphosphatidylcholine is highly sensitive to hydration: phospholipid polymorphism induced by molecular rearrangement in the headgroup region. *Biophys. J.* 73:870–877.

86. McGaughey, G. B., M. Gagné, and A. K. Rappé. 1998. pi-Stacking interactions. Alive and well in proteins. *J. Biol. Chem.* 273:15458–15463.

87. Moser, M., S. Panahandeh, …, M. Müller. 2007. In vitro analysis of the bacterial twin-arginine-dependent protein export. *Methods Mol. Biol.* 390:63–79.

88. Sharpe, H. J., T. J. Stevens, and S. Munro. 2010. A comprehensive comparison of transmembrane domains reveals Organelle-specific properties. *Cell.* 142:158–169.

89. Pogozheva, I. D., S. Tristram-Nagle, …, A. L. Lomize. 2013. Structural adaptations of proteins to different biological membranes. *Biochim. Biophys. Acta.* 1828:2592–2608.

90. Saidijam, M., S. Azizpour, and S. G. Patching. 2018. Comprehensive analysis of the numbers, lengths and amino acid compositions of transmembrane helices in prokaryotic, eukaryotic and viral integral membrane proteins of high-resolution structure. *J. Biomol. Struct. Dyn.* 36:443–464.

91. Harzer, U., and B. Bechinger. 2000. Alignment of lysine-anchored membrane peptides under conditions of hydrophobic mismatch: a CD, 15N and 31P solid-state NMR spectroscopy investigation. *Biochemistry.* 39:13106–13114.

92. Killian, J. A. 2003. Synthetic peptides as models for intrinsic membrane proteins. *FEBS Lett.* 555:134–138.

93. Kubyshkin, V., S. L. Grage, …, N. Budisa. 2019. Bilayer thickness determines the alignment of model polyproline helices in lipid membranes. *Phys. Chem. Chem. Phys.* 21:22396–22408.

94. Kubyshkin, V., S. L. Grage, …, N. Budisa. 2018. Transmembrane polyproline helix. *J. Phys. Chem. Lett.* 9:2170–2174.

95. Hao, B., W. Zhou, and S. M. Theg, Functional analysis of the polar amino acid in TatA transmembrane helix. Preprint at bioRxiv, doi: 10.1101/2021.11.30.470661.

96. Bechinger, B. 1996. Towards membrane protein design: pH-sensitive topology of histidine-containing polypeptides. *J. Mol. Biol.* 263:768–775.

97. Caputo, G. A., and E. London. 2004. Position and ionization state of Asp in the core of membrane-inserted α helices control both the equilibrium between transmembrane and nontransmembrane helix topography and transmembrane helix positioning. *Biochemistry.* 43:8794–8806.

98. Caputo, G. A., and E. London. 2003. Cumulative effects of amino acid substitutions and hydrophobic mismatch upon the transmembrane stability and conformation of hydrophobic α-helices. *Biochemistry.* 42:3275–3285.

99. Lew, S., J. Ren, and E. London. 2000. The effects of polar and/or ionizable residues in the core and flanking regions of hydrophobic helices on transmembrane conformation and oligomerization. *Biochemistry.* 39:9632–9640.

100. Krishnakumar, S. S., and E. London. 2007. Effect of sequence hydrophobicity and bilayer width upon the minimum length required for the formation of transmembrane helices in membranes. *J. Mol. Biol.* 374:671–687.

101. Shahidullah, K., and E. London. 2008. Effect of lipid composition on the topography of membrane-associated hydrophobic helices: stabilization of transmembrane topography by anionic lipids. *J. Mol. Biol.* 379:704–718.

102. Ren, J., S. Lew, …, E. London. 1997. Transmembrane orientation of hydrophobic α-helices is regulated both by the relationship of helix length to bilayer thickness and by the cholesterol concentration. *Biochemistry.* 36:10213–10220.

103. Weerakkody, D., A. Moshnikova, …, Y. K. Reshetnyak. 2013. Family of pH (low) insertion peptides for tumor targeting. *Proc. Natl. Acad. Sci. USA.* 110:5834–5839.

104. Fendos, J., F. N. Barrera, and D. M. Engelman. 2013. Aspartate embedding depth affects pHLIP's insertion pKa. *Biochemistry.* 52:4595–4604.

105. Barrera, F. N., D. Weerakkody, …, D. M. Engelman. 2011. Roles of carboxyl groups in the transmembrane insertion of peptides. *J. Mol. Biol.* 413:359–371.

106. Andreev, O. A., A. G. Karabadzhak, …, Y. K. Reshetnyak. 2010. pH (low) insertion peptide (pHLIP) inserts across a lipid bilayer as a helix and exits by a different path. *Proc. Natl. Acad. Sci. USA.* 107:4081–4086.

107. Reshetnyak, Y. K., M. Segala, …, D. M. Engelman. 2007. A monomeric membrane peptide that lives in three worlds: in solution, attached to, and inserted across lipid bilayers. *Biophys. J.* 93:2363–2372.

108. Andreev, O. A., A. D. Dupuy, …, Y. K. Reshetnyak. 2007. Mechanism and uses of a membrane peptide that targets tumors and other acidic tissues in vivo. *Proc. Natl. Acad. Sci. USA.* 104:7893–7898.

109. Young, R. 2013. Phage lysis: do we have the hole story yet? *Curr. Opin. Microbiol.* 16:790–797.

110. Pang, T., T. Park, and R. Young. 2010. Mapping the pinhole formation pathway of S21. *Mol. Microbiol.* 78:710–719.

111. Pang, T., T. Park, and R. Young. 2010. Mutational analysis of the S21 pinholin. *Mol. Microbiol.* 76:68–77.

112. Park, T., D. K. Struck, …, R. Young. 2006. Topological dynamics of holins in programmed bacterial lysis. *Proc. Natl. Acad. Sci. USA.* 103:19713–19718.

113. Pang, T., T. C. Fleming, …, R. Young. 2013. Visualization of pinholin lesions in vivo. *Proc. Natl. Acad. Sci. USA.* 110:E2054–E2063.

114. Pang, T., C. G. Savva, …, R. Young. 2009. Structure of the lethal phage pinhole. *Proc. Natl. Acad. Sci. USA.* 106:18966–18971.

115. Steger, L. M. E., A. Kohlmeyer, …, A. S. Ulrich. 2020. Structural and functional characterization of the pore-forming domain of pinholin $S^{21}68$. *Proc. Natl. Acad. Sci. USA.* 117:29637–29646.

116. Fujita, K., S. S. Krishnakumar, …, E. Wimmer. 2007. Membrane topography of the hydrophobic anchor sequence of poliovirus 3A and 3AB proteins and the functional effect of 3A/3AB membrane association upon RNA replication. *Biochemistry.* 46:5185–5199.

117. Vitrac, H., D. M. MacLean, …, W. Dowhan. 2015. Dynamic membrane protein topological switching upon changes in phospholipid environment. *Proc. Natl. Acad. Sci. USA.* 112:13874–13879.

118. Rather, P. 2013. Role of rhomboid proteases in bacteria. *Biochim. Biophys. Acta.* 1828:2849–2854.

119. Fritsch, M. J., M. Krehenbrink, …, T. Palmer. 2012. Processing by rhomboid protease is required for Providencia stuartii TatA to interact with TatC and to form functional homo-oligomeric complexes. *Mol. Microbiol.* 84:1108–1123.

120. Stevenson, L. G., K. Strisovsky, …, P. N. Rather. 2007. Rhomboid protease AarA mediates quorum-sensing in Providencia stuartii by activating TatA of the twin-arginine translocase. *Proc. Natl. Acad. Sci. USA.* 104:1003–1008.

121. Frielingsdorf, S., M. Jakob, and R. B. Klösgen. 2008. A stromal pool of TatA promotes Tat-dependent protein transport across the thylakoid membrane. *J. Biol. Chem.* 283:33838–33845.

122. Pop, O. I., M. Westermann, …, J. P. Müller. 2003. Sequence-specific binding of prePhoD to soluble TatAd indicates protein-mediated targeting of the Tat export in Bacillus subtilis. *J. Biol. Chem.* 278:38428–38436.

123. Berthelmann, F., D. Mehner, …, T. Brüser. 2008. Recombinant expression of tatABC and tatAC results in the formation of interacting cytoplasmic TatA tubes in Escherichia coli. *J. Biol. Chem.* 283:25281–25289.

124. De Keersmaeker, S., K. Vrancken, …, N. Geukens. 2007. The Tat pathway in Streptomyces lividans: interaction of Tat subunits and their role in translocation. *Microbiology.* 153 (Pt 4):1087–1094.

125. Schreiber, S., R. Stengel, …, J. P. Müller. 2006. Affinity of TatCd for TatAd elucidates its receptor function in the Bacillus subtilis twin arginine translocation (Tat) translocase system. *J. Biol. Chem.* 281:19977–19984.

126. Taubert, J., B. Hou, …, T. Brüser. 2015. TatBC-independent TatA/tat substrate interactions contribute to transport efficiency. *PLoS One.* 10:e0119761.

127. De Keersmaeker, S., L. Van Mellaert, …, N. Geukens. 2005. Functional analysis of TatA and TatB in streptomyces lividans. *Biochem. Biophys. Res. Commun.* 335:973–982.

128. De Keersmaeker, S., L. Van Mellaert, …, N. Geukens. 2005. Structural organization of the twin-arginine translocation system in Streptomyces lividans. *FEBS Lett.* 579:797–802.

129. Koch, S., M. J. Fritsch, …, T. Palmer. 2012. Escherichia coli TatA and TatB proteins have N-out, C-in topology in intact cells. *J. Biol. Chem.* 287:14420–14431.

130. Alami, M., D. Trescher, …, M. Müller. 2002. Separate analysis of twin-arginine translocation (Tat)-specific membrane binding and translocation in Escherichia coli. *J. Biol. Chem.* 277:20499–20503.

131. Wien, F., and B. A. Wallace. 2005. Calcium fluoride micro cells for synchrotron radiation circular dichroism spectroscopy. *Appl. Spectrosc.* 59:1109–1113.

132. Clarke, D. T., and G. Jones. 2004. CD12: a new high-flux beamline for ultraviolet and vacuum-ultraviolet circular dichroism on the SRS. *J. Synchrotron Radiat.* 11:142–149.

133. Lees, J. G., B. R. Smith, …, B. A. Wallace. 2004. CDtool—an integrated software package for circular dichroism spectroscopic data processing, analysis, and archiving. *Anal. Biochem.* 332:285–289.

134. Kelly, S. M., T. J. Jess, and N. C. Price. 2005. How to study proteins by circular dichroism. *Biochim. Biophys. Acta.* 1751:119–139.

135. Levitt, M. H., D. Suter, and R. R. Ernst. 1986. Spin dynamics and thermodynamics in solid-state NMR cross polarization. *J. Chem. Phys.* 84:4243–4255.

136. Metz, G., X. L. Wu, and S. O. Smith. 1994. Ramped-amplitude cross polarization in magic-angle-spinning NMR. *J. Magn. Reson., Ser. A.* 110:219–227.

137. Sinha, N., C. V. Grant, …, S. J. Opella. 2005. SPINAL modulated decoupling in high field double- and triple-resonance solid-state NMR experiments on stationary samples. *J. Magn. Reson.* 177:197–202.

138. Fung, B. M., A. K. Khitrin, and K. Ermolaev. 2000. An improved broadband decoupling sequence for liquid crystals and solids. *J. Magn. Reson.* 142:97–101.

139. Lindorff-Larsen, K., S. Piana, …, D. E. Shaw. 2010. Improved side-chain torsion potentials for the Amber ff99SB protein force field. *Proteins.* 78:1950–1958.

140. Strunk, T., M. Wolf, …, W. Wenzel. 2012. Simona 1.0: an efficient and versatile framework for stochastic simulations of molecular and nanoscale systems. *J. Comput. Chem.* 33:2602–2613.

141. Setzler, J., C. Seith, …, W. Wenzel. 2014. SLIM: an improved generalized Born implicit membrane model. *J. Comput. Chem.* 35:2027–2039.

142. Spassov, V. Z., L. Yan, and S. Szalma. 2002. Introducing an implicit membrane in generalized born/solvent accessibility continuum solvent models. *J. Phys. Chem. B.* 106:8726–8738.

143. Tanizaki, S., and M. Feig. 2005. A generalized Born formalism for heterogeneous dielectric environments: application to the implicit modeling of biological membranes. *J. Chem. Phys.* 122:124706–124713.

144. Still, W. C., A. Tempczyk, …, T. Hendrickson. 1990. Semianalytical treatment of solvation for molecular mechanics and dynamics. *J. Am. Chem. Soc.* 112:6127–6129.

145. Brieg, M., and W. Wenzel. 2013. PowerBorn: a barnes–hut tree implementation for accurate and efficient Born radii computation. *J. Chem. Theory Comput.* 9:1489–1498.

146. Blümmel, A. S., L. A. Haag, …, J. Fröbel. 2015. Initial assembly steps of a translocase for folded proteins. *Nat. Commun.* 6:7234.

147. Larkin, M. A., G. Blackshields, …, D. G. Higgins. 2007. Clustal W and clustal X version 2.0. *Bioinformatics.* 23:2947–2948.

148. Waterhouse, A. M., J. B. Procter, …, G. J. Barton. 2009. Jalview Version 2--a multiple sequence alignment editor and analysis workbench. *Bioinformatics.* 25:1189–1191.

Biophysical Journal, Volume *122*

Supplemental information

Length matters: Functional flip of the short TatA transmembrane helix

Eva R. Stockwald, Lena M.E. Steger, Stefanie Vollmer, Christina Gottselig, Stephan L. Grage, Jochen Bürck, Sergii Afonin, Julia Fröbel, Anne-Sophie Blümmel, Julia Setzler, Wolfgang Wenzel, Torsten H. Walther, and Anne S. Ulrich

This PDF file includes:

Table S 1 Template plasmids and primers for the construction of the TatA constructs

TatA mutant	plasmid	template plasmid	forward primer	reverse primer
$TatA_{2-45}$ ΔLIL	pET28 $TatA_{1-45}$ ΔLIL	pET28 $TatA_{1-45}$	5'-GA ATA CCG GGC ATC TTC GTC ATC GC-3'	5'-GC GAT GAC GAA GAT GCC CGG TAT TC-3'
$TatA_{2-45}$ LAL	pET28 $TatA_{1-45}$ LAL	pET28 $TatA_{1-45}$	5'-GGC TTG ATT CTC CTG GCG TTG ATC TTC GTC ATC-3'	5'-GAT GAC GAA GAT CAA CGC CAG GAG AAT CAA GCC-3'
$TatA_{2-45}$ LALAL	pET28 $TatA_{1-45}$ LALAL	pET28 $TatA_{1-45}$	5'-GGC TTG ATT CTC CTG GCG TTG GCC CTG ATC TTC GTC ATC-3'	5'-GAT GAC GAA GAT CAG GGC CAA CGC CAG GAG AAT CAA GCC-3'
$TatA_{2-45}$ LALALAL	pET28 $TatA_{1-45}$ LALALAL	pET28 $TatA_{1-45}$	5'-GGC TTG ATT CTC CTG GCG TTG GCC CTG GCG TTG ATC TTC GTC ATC-3'	5'-GAT GAC GAA GAT CAA CGC CAG GGC CAA CGC CAG GAG AAT CAA GCC-3'
$TatA_{2-45}$ F_2D	pET28 $TatA_{1-45}$ F_2D	pET28 $TatA_{1-45}$	5'-CGC GGC AGC CAT ATG GAT TCA AAC ATT GGA ATA CCG-3'	5'-CGG TAT TCC AAT GTT TGA ATC CAT ATG GCT GCC GCG-3'
$TatA_{2-45}$ F_2D I_7D	pET28 $TatA_{1-45}$ F_2D I_7D	pET28 $TatA_{1-45}$ F_2D	5'-GAT TCA AAC ATT GGA GAT CCG GGC TTG ATT CTC-3'	5'-GAG AAT CAA GCC CGG ATC TCC AAT GTT TGA ATC-3'
E. coli TatA LAL	pET22b+TatA LAL BCD	pET22b+TatABCD	5'-GT ATT TGG CAG TTA TTG ATT CTG GCG TTG ATT GCC GTC ATC GTT GTA C-3'	5'-G TAC AAC GAT GAC GGC AAT CAA CGC CAG AAT CAA TAA CTG CCA AAT AC-3'
E. coli TatA LALA	pET22b+TatA LALA BCD	pET22b+TatABCD	5'-GT ATT TGG CAG TTA TTG ATT CTG GCG TTG GCC ATT GCC GTC ATC GTT GTA C-3'	5'-G TAC AAC GAT GAC GGC AAT GGC CAA CGC CAG AAT CAA TAA CTG CCA AAT AC-3'
E. coli TatA LALALAL	pET22b+TatA LALALAL BCD	pET22b+TatABCD	5'-GT ATT TGG CAG TTA TTG ATT CTG GCG TTG GCC CTG GCG TTG ATT GCC GTC ATC GTT GTA C-3'	5'-G TAC AAC GAT GAC GGC AAT CAA CGC CAG GGC CAA CGC CAG AAT CAA TAA CTG CCA AAT AC-3'

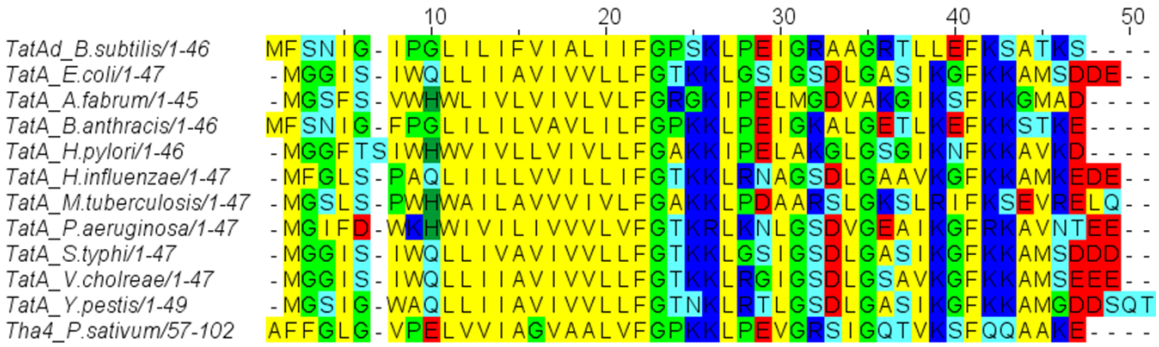

Figure S1: Sequence alignment of TatA from different organisms. Only the sequences of the TMH and APH are shown (the sequence of *P. sativum* is additionally N-terminally truncated). The sequence alignment proves that the unusual short length of the TatA TMH is highly conserved. The colors illustrate the different types of residues: yellow - hydrophobic (Leu, Ile, Val, Phe, Ala, Met, Trp); red - anionic (Asp, Glu); blue - cationic (Lys, Arg); light blue - polar (Ser, Thr, Gln, Asn, Tyr, Cys); light green - helix modifiers (Pro, Gly); dark green - ionizable (His). Data were created using the software Clustal [147] and Jalview [148].

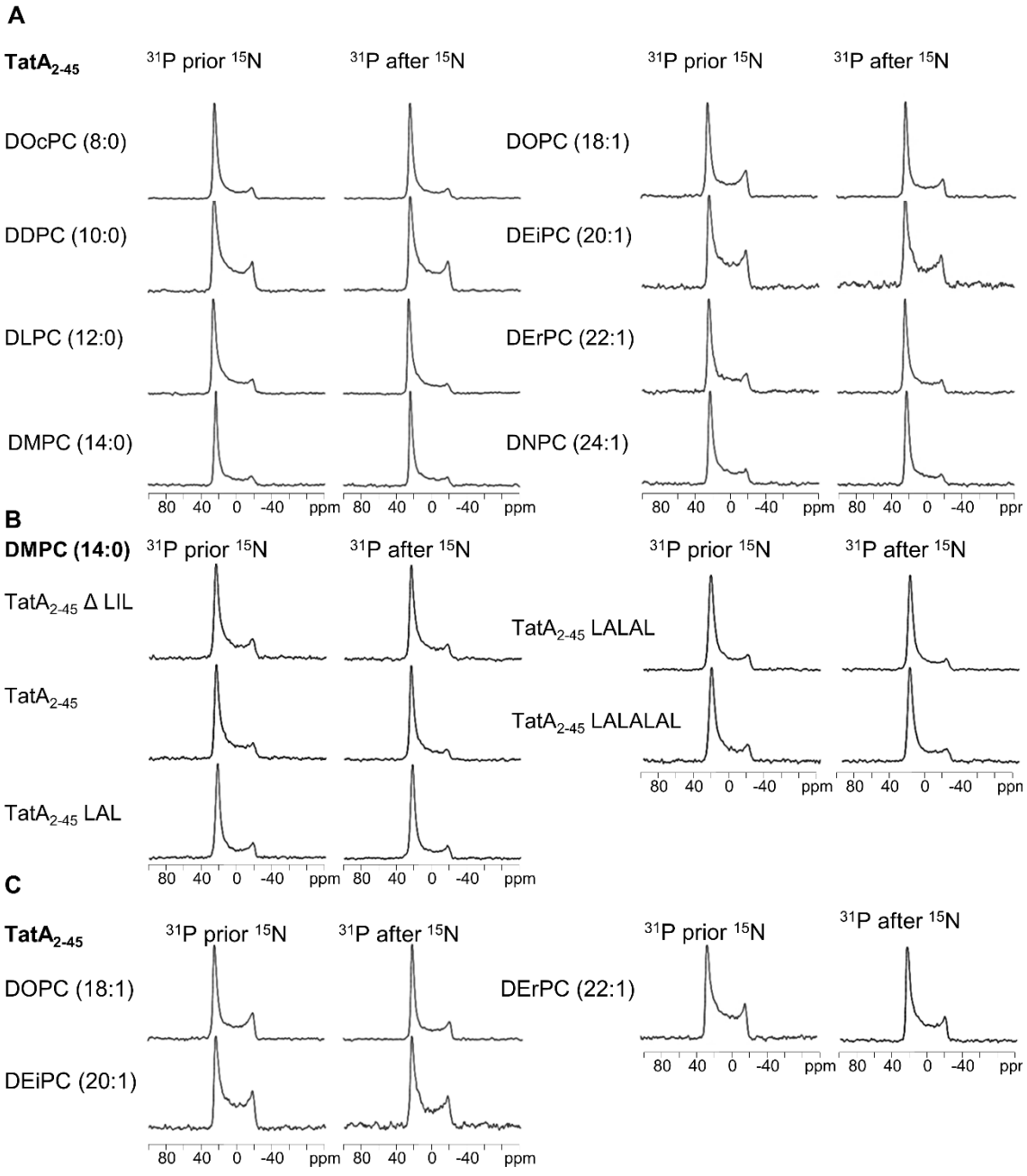
A
TatA2-45
31P prior 15N
31P after 15N
31P prior 15N
31P after 15N
DOcPC (8:0)
DOPC (18:1)
DDPC (10:0)
DEiPC (20:1)
DLPC (12:0)
DErPC (22:1)
DMPC (14:0)
DNPC (24:1)
80 40 0 -40 ppm
B
DMPC (14:0)
31P prior 15N
31P after 15N
31P prior 15N
31P after 15N
TatA2-45 Δ LIL
TatA2-45 LALAL
TatA2-45
TatA2-45 LALALAL
TatA2-45 LAL
C
TatA2-45
31P prior 15N
31P after 15N
31P prior 15N
31P after 15N
DOPC (18:1)
DErPC (22:1)
DEiPC (20:1)

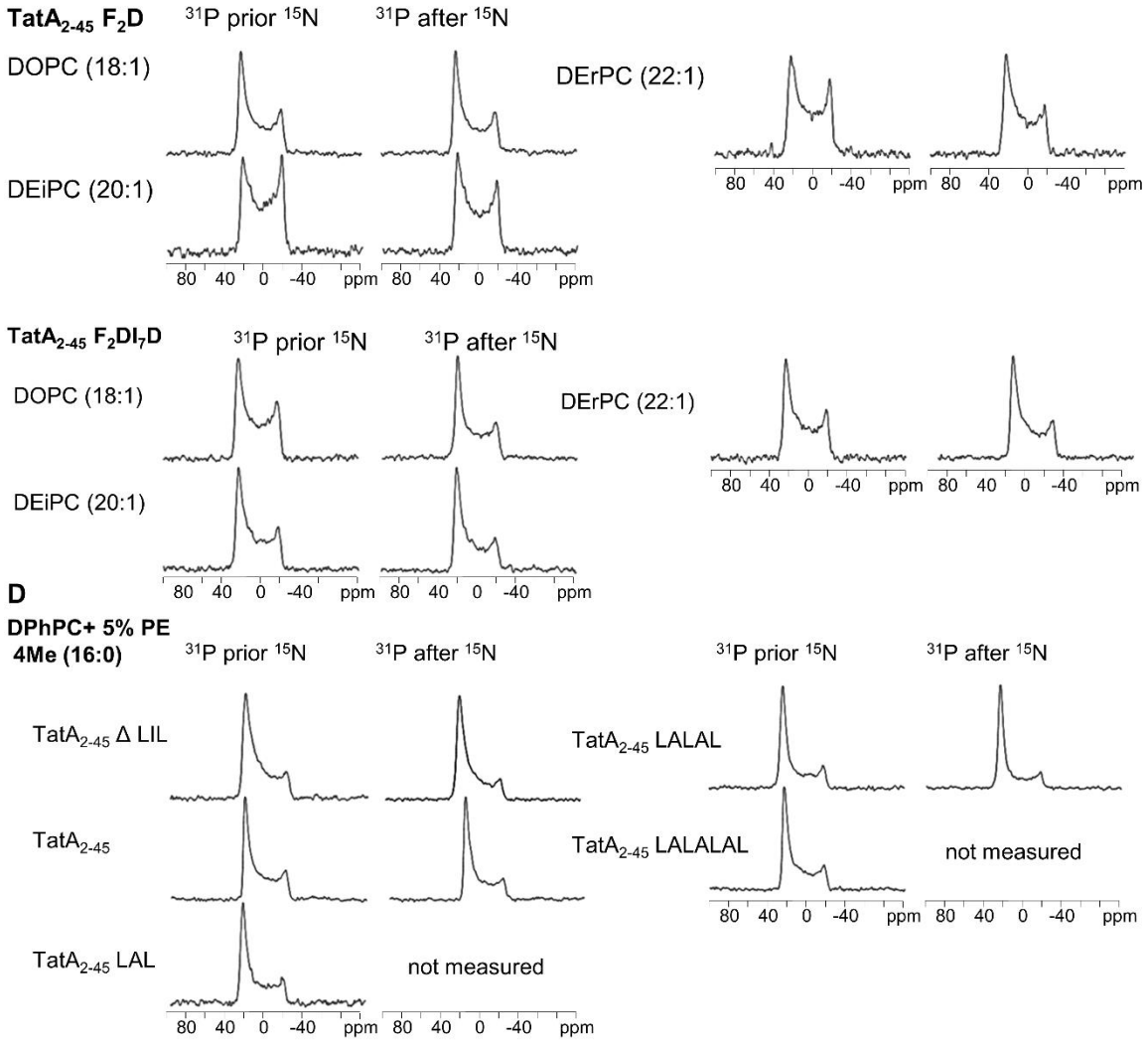

Figure S2: ^{31}P-NMR spectra before and after the ^{15}N-NMR measurements. One-dimensional solid-state ^{31}P-NMR spectra were recorded to assess the quality of the lipid alignment and any potential sample degradation. NMR measurements were performed using the standard sample orientation in which the bilayer normal is aligned parallel to the static magnetic field. **(A)** The uniformly ^{15}N-labelled $TatA_{2-45}$ wild type was reconstituted in macroscopically aligned phosphatidylcholine bilayers with varying membrane thickness, composed of DOcPC, DDPC, DLPC, DMPC, DOPC, DEiPC, DErPC, and DNPC (corresponding to Fig. 2). **(B)** $TatA_{2-45}$ variants with an extended or shortened TMH were reconstituted in macroscopically aligned lipid bilayers composed of DMPC (corresponding to Fig. 3). **(C)** $TatA_{2-45}$ variants with varying N-terminal charge density were reconstituted in macroscopically aligned lipid bilayers composed of DOPC, DEiPC and DErPC (corresponding to Fig. 4). **(D)** $TatA_{2-45}$ variants with an extended or shortened TMH were reconstituted in branched phytanoyl lipids composed of a mixture of DPhPC/DPhPE (95/5 mol/mol) (corresponding to Fig. 5).

The spectral lineshape is composed of a superposition of the aligned lamellar phase (narrow signal at around 30 ppm, which arises due to the parallel alignment of the phospholipids to the magnetic field) and an upfield powder content, which is exceptionally pronounced only for the N-terminally charged variants. The ^{31}P-NMR spectra show that the 14-22 hour ^{15}N-NMR experiments had no perturbing effect on the orientation of the macroscopically aligned membranes in general.

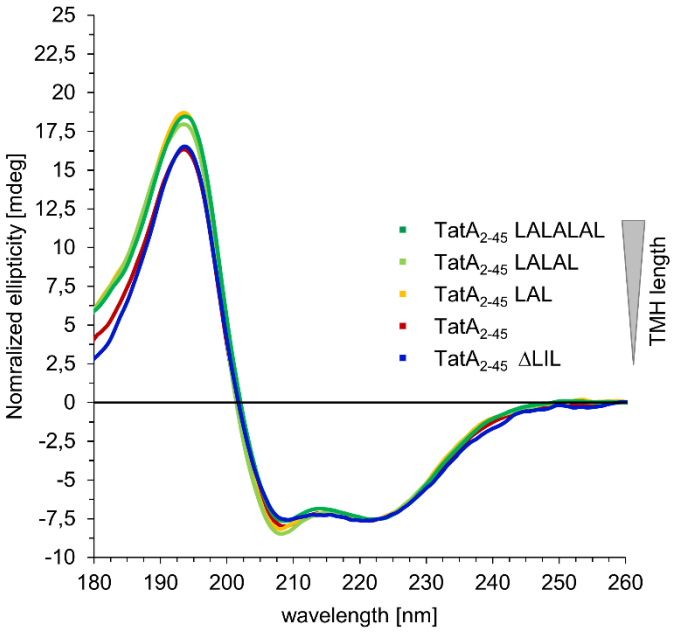

Figure S3: SRCD spectra of $TatA_{2-45}$ and $TatA_{2-45}$ variants with an extended or shortened TMH reconstituted in DMPC vesicles. All proteins were reconstituted in DMPC vesicles with a peptide to lipid ration of 1:50. For direct comparison, the spectra were normalized at 223 nm. All spectra show a typical α-helical line shape with characteristic bands at around 194 nm, 209 nm and 223 nm.

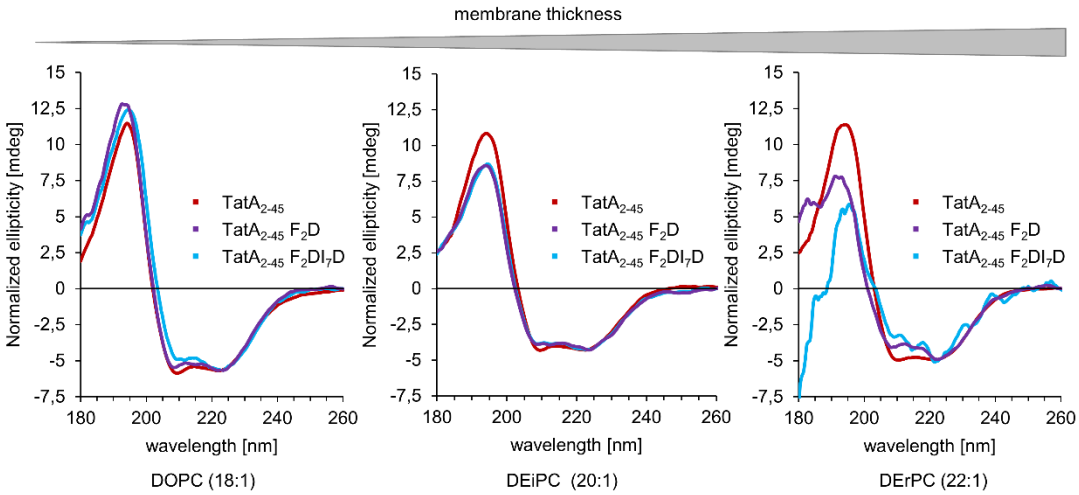

Figure S4: SRCD spectra of $TatA_{2-45}$ and $TatA_{2-45}$ variants with an N-terminal charge reconstituted DOPC, DEiPC and DErPC vesicles. All proteins were reconstituted with peptide to lipid ration of 1:50. For direct comparison, the spectra were normalized at 223 nm. All spectra show a typical α-helical line shape with characteristic bands at around 194 nm, 209 nm and 223 nm. In DEiPC $TatA_{2-45}$ F_2D and $TatA_{2-45}$ F_2DI_7D start to show some amount of absorption flattening, which is in DErPC strongly pronounced. This behaviour is consistent with the observed protein aggregation in ^{15}N-NMR.

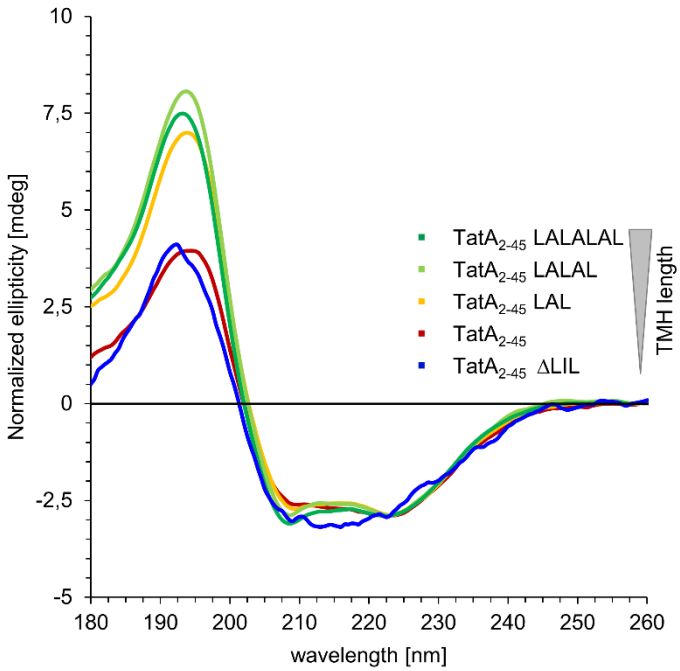

Figure S5: SRCD spectra of $TatA_{2-45}$ and $TatA_{2-45}$ variants with an extended or shortened TMH reconstituted in DPhPC/DPhPE (95/5 mol/mol) vesicles. All proteins were reconstituted in mixture of DPhPC/DPhPE (95/5 mol/mol) with a peptide to lipid ratio of 1:50. For direct comparison, the spectra were normalized at 223 nm. All spectra show a typical α-helical line shape with characteristic bands at around 194 nm, 209 nm and 223 nm. The variants with extended TMHs possess a larger α-helical content.

Supplemental References

[147] Larkin, M. A., Blackshields, G., Brown, N. P., Chenna, R., McGettigan, P. A., McWilliam, H., Valentin, F., Wallace, I. M., Wilm, A., Lopez, R., Thompson, J. D., Gibson, T. J. and Higgins, D. G. 2007. Clustal W and Clustal X version 2.0. *Bioinformatics* 23 (21): 2947-2948.

[148] Waterhouse, A. M., Procter, J. B., Martin, D. M. A., Clamp, M. and Barton, G. J. 2009. Jalview Version 2--a multiple sequence alignment editor and analysis workbench. *Bioinformatics* 25 (9): 1189-1191.